Andean Geology 41 (1): 49-82. January, 2014
doi: 10.5027/andgeoV41n1-a03

Andean Geology
formerly Revista Geológica de Chile
www.andeangeology.cl

U-Pb Geochronology and Hf-O Isotopes of zircons from the Pennsylvanian Coastal Batholith, South-Central Chile

Katja Deckart[1], Francisco Hervé[1, 2], C. Mark Fanning[3], Valeria Ramírez[1], Mauricio Calderón[1], Estanislao Godoy[1]

[1] *Departamento de Geología, Universidad de Chile. Plaza Ercilla 803, Santiago, Chile.*
kdeckart@cec.uchile.cl; mccaldera@gmail.com; egodoyster@gmail.com; valramirezm.82@outlook.com
[2] *Escuela de Ciencias de la Tierra, Universidad Andrés Bello, Sazié 2315. Santiago, Chile.*
fherve@unab.cl
[3] *Research School of Earth Sciences, The Australian National University, Canberra 0200, Australia.*
mark.fanning@anu.edu.au

ABSTRACT. The Coastal Batholith of south-central Chile between latitudes 33° and 40°S is composed of calc-alkaline granitoids emplaced in a relatively restricted time period. New SHRIMP U-Pb zircon ages on eight quartzdioritic to granitic rocks collected over a distance of 800 km yielded ages between 300 and 320 Ma, Pennsylvanian (late Carboniferous). Lu-Hf isotopic analyses on the same zircon grains have initial $\varepsilon Hf_{(i)}$ values from +1.67 to -5.64. The $\delta^{18}O$ ratios for that grains range from 6.4 to 8.6‰. These new isotopic data point to a relative homogeneous source with prominent components of the continental crust. The calculated Mesoproterozoic Depleted Mantel model ages, in addition to the short span of intrusive ages give insights to the position of the proto-Gondwana margin and the changing subduction mechanism at the end of late Paleozoic time.

Keywords: Coastal Batholith, Pennsylvanian, zircons, U-Pb, Lu-Hf and O isotope geochemistry.

RESUMEN. Geocronología U-Pb e isótopos de Hf-O en circones del batolito de la Costa Pensilvaniana, Chile. El Batolito de la costa de Chile central-sur entre las latitudes 33° y 40°S se compone de granitoides calcoalcalinos y se ha emplazado en un período de tiempo relativamente restringido. Nuevas edades U-Pb SHRIMP en circones de ocho rocas graníticas a cuarzo-dioríticas, las que representan un muestreo a lo largo de 800 km, entregaron edades entre 300 y 320 Ma, Pensilvaniano (Carbonífero tardío). Análisis isotópicos de Lu-Hf en los mismos granos de circón han entregados valores isotópicos iniciales de $\varepsilon Hf_{(i)}$ desde +1,67 a -5,64. La razón $\delta^{18}O$ para esos granos varía desde 6,4 a 8,6‰. Estos nuevos datos isotópicos apuntan a una fuente relativamente homogénea con importantes componentes de la corteza continental. Las edades modelos de Manto Empobrecido calculadas del Mesoproterozoico en conjunto con el intervalo de edades restringidas de los intrusivos dan información respeto de la posición del protomargen del continente de Gondwana y a las variaciones en el mecanismo de la subducción al final del Paleozoico tardío.

Palabras clave: Batolito de la Costa, Pensilvaniano, Circones, Geoquímica isotópica de U-Pb, Lu-Hf y O.

1. Introduction

The Chilean Coastal Cordillera (33°-40°S) comprises a distinctive lithotectonic association representative of subduction zone processes. Critically important indicators of subduction are the late Paleozoic accretionary complex and the calc-alkaline Coastal Batholith. Although their origin within a subduction setting as exemplified for the Neogene Chilean active margin (*e.g.,* Barazangi and Isacks, 1976; Hager and O'Connell, 1978; Jordan *et al*., 1983; Cahill and Isacks, 1992) seems straightforward (Hervé *et al*., 1988; Hervé *et al*., 2007a; Parada *et al*., 2007), the exact timing, nature and geodynamic significance of the Coastal Batholith in south-central Chile warrants further detailed investigations.

The Coastal Batholith is a large and elongate composite intrusive body within slightly older metamorphic rocks of the accretionary prism (Hervé *et al*., 2013). The sedimentary protolith of these country rocks was deposited and then shortly after buried to a depth of about 8 to 10 km (at about 3 kbar; Willner *et al*., 2005) where it was intruded by quartzdioritic to granitic magmas. Trench-ward shift of arc magmatism from an easterly location apparently occurred as Mississippian (early Carboniferous) detrital zircons are present in the sedimentary rocks of the accretionary prism (Hervé *et al*., 2013). This shift may be explained by global tectonic plate reorganization, or tectonic processes such as the steepening of the subducted oceanic slab due to subduction of older and colder oceanic lithosphere. Other possible geodynamic scenarios (*e.g.,* subduction rollback), however, are explored.

In this study we report new SHRIMP U-Pb zircon ages on distinct portions of the largely north-south elongated Paleozoic Coastal Batholith and the first Hf-O isotope data for this batholith. The aim is to present new aspects to the timing and petrogenesis of the batholith and magmatism along this portion of the proto-Pacific Gondwana margin. Our goal is to demonstrate that the Coastal Batholith was emplaced in a short period of time and shows different petrogenetic features compared to those other cordilleran batholiths which were formed along tens or hundred million years through multiple pulses of magmatism (cf. Hervé *et al*., 2007b).

2. Geologic Background

The Coastal Batholith of south-central Chile crops out to the east of the accretionary metamorphic complex between 33°S and 38°20'S, jumping at 40°S further east into the Principal Cordilleran range (Fig. 1).

The accretionary complex is subdivided into two metamorphic series with distinct P/T conditions (Godoy, 1970; Aguirre *et al*., 1972). The high P-low T Western and the low P-high T Eastern Series (Hervé, 1977; Willner *et al*., 2005) located to the north of 40ºS have Carboniferous depositional ages (Hervé *et al*., 2013). The Eastern Series shows a metamorphic overprint at around 300 Ma (Willner *et al*., 2005) which is related to the intrusive event of the Coastal Batholith on its eastern side. To the south of 40ºS the Western Series shows a Permian depositional age and Permian to Triassic age range for metamorphism (Duhart *et al*., 2001; Hervé *et al*., 2013).

The Coastal Batholith is composed of calc-alkaline granitoid suites developed during late Paleozoic time, mainly between late Carboniferous and Early Permian (*e.g.,* Cordani *et al*., 1976; Hervé, 1976; Hervé *et al*., 1988; Parada *et al*., 1991; Martin *et al*., 1999a; Ramírez, 2010). Also present in the Coastal Cordillera are gabbros and fayalite-bearing granites of Triassic age and classified as an anorogenic A-type granitoid suite (Vásquez and Franz, 2008) and some late to middle Jurassic two-pyroxene diorites, gabbros and hornblende-biotite tonalites (Godoy and Loske, 1988; Parada *et al*., 1991; Hernández, 2006).

Furthermore, the subduction related plutonic event represented by the Subcordilleran Batholith in Patagonia, Argentina, indicates ages of the Triassic-Jurassic boundary (Rapela *et al*., 2003).

3. Previous age and isotopic data of the late Paleozoic Coastal Batholith

The Coastal Batholith intrusives 30 km north of the Quintay study area at Reñaca, yielded a Rb-Sr isochron age of 299±31 Ma (Hervé *et al*., 1988). At Valparaíso, 10 km to the south of Reñaca, a Rb-Sr isochron age of 296±5 Ma (Shibata *et al*., 1984) was obtained. South of Quintay, at Algarrobo, an age of 292±2 Ma and at Santo Domingo an age of 308±15 Ma was published by Hervé *et al*. (1988). Both represent ages of the northern part or the out-

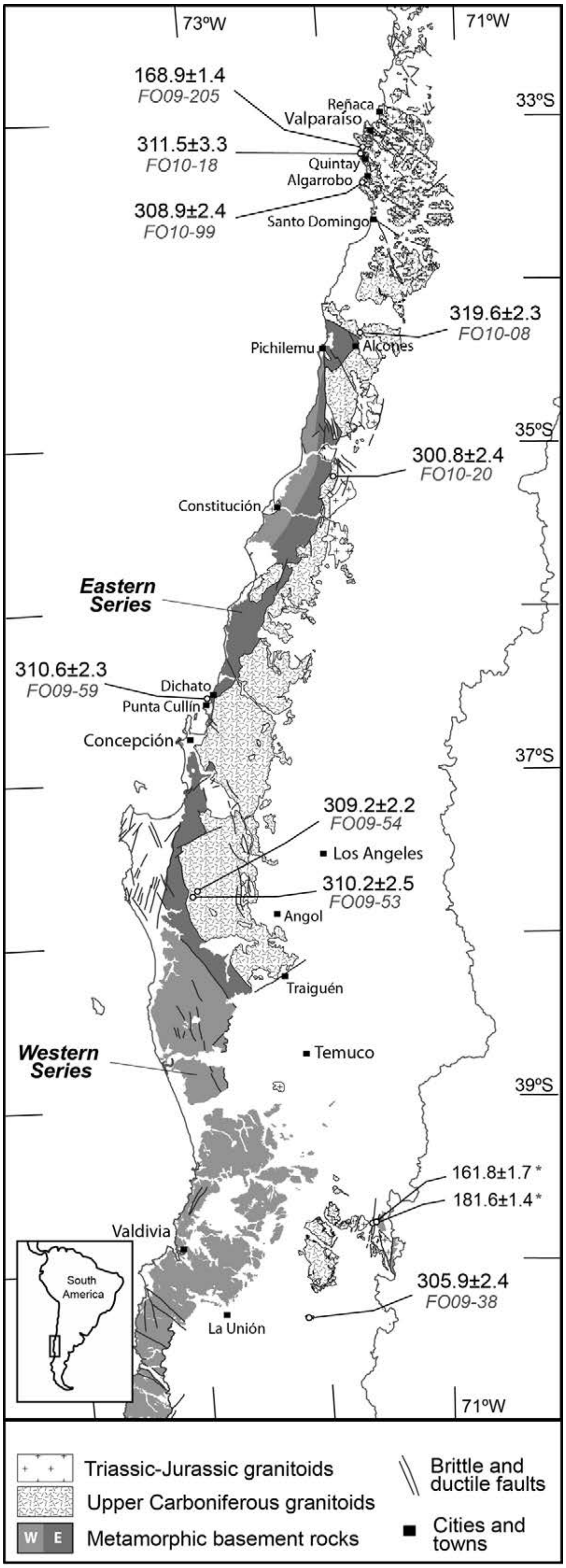

cropping Coastal Batholith. For the same dated samples $^{87}Sr/^{86}Sr$ whole rock initial ratios range between 0.70582 and 0.70605. Earlier, Cordani *et al*. (1976) presented a late Paleozoic age of 319±17 Ma (K-Ar recalculated) and a Juarssic age of 169±12 Ma (K-Ar recalculated) at Quintay. The Paleozoic sample yields an initial $^{87}Sr/^{86}Sr$ isotope ratio of 0.7132, the Jurassic sample is less radiogenic with an initial ratio of 0.7038. Two more Paleozoic K-Ar ages are presented in Hervé *et al*. (1988) for Algarrobo intrusives on biotite and hornblende yielding 287±7 Ma and 296±7 Ma, respectively. At Quintay and Reñaca, two further Jurassic ages on biotite are published (Hervé *et al*., 1988), at 159±4 Ma and 156±1 Ma, respectively. An additional whole rock Rb-Sr age was likewise obtained yielding 167±14 Ma with an initial $^{87}Sr/^{86}Sr$ whole rock isotope ratio of 0.70412. Furthermore, Gana *et al.* (1996) and Wall *et al.* (1996) published for the coastal area between Valparaíso and Cartagena several Middle to Late Jurassic K-Ar mineral ages on plutonic rock units. The Jurassic ages were attributed to thermal rejuvenation in rocks associated to the intrusion of Jurassic bodies.

A U-Pb zircon crystallization age of 299±10 Ma for the Pomaire pluton further east (Gana and Tosdal, 1996), inland of Quintay, confirms the strong presence of Carboniferous (Pennsylvanian) rocks in this area (Cochoa Unit after Rivano *et al*. (1993). Earlier, Godoy and Loske (1988) published two U-Pb dates on zircon fractions in two distinct localities at Quintay; dates are 290 Ma (tonalite) and 309 Ma (gneissic granite). Additionally, Gana and Tosdal (1996) obtained a U-Pb zircon age of 214±1 Ma (Late Triassic) from the Cartagena gneissic diorite unit at Punta Suspiro, directly north of San Antonio harbor, about 25 km south of Algarrobo.

FIG. 1. Geological sketch map of central Chile between 33° and 40°S (modified from SERNAGEOMIN, 2003). Patterned zone represents the Coastal Batholith and rocks of the accretionary metamorphic prism. Additional age data are U-Pb zircon crystallization ages (*) of the plutonic protolith of gneisses from the main trace of the Liquiñe-Ofqui fault zone Hervé *et al*., 2013).

Hervé *et al.* (1988) published a late Carboniferous, Pennsylvanian age for a coastal Santo Domingo granite sample, some 35 km south of Algarrobo. The Rb-Sr age is 308±15 Ma, with a whole rock initial $^{87}Sr/^{86}Sr$ isotope ratio of 0.70582.

Further to the south, *ca.* 35 km northeast from the city of Concepción at the Dichato locality, a K-Ar biotite age of 306±6 Ma was published (Hervé *et al*., 1988). The same age (Rb-Sr isochron of 306±6 Ma) was obtained by Lucassen *et al.* (2004) in a diorite from the Cantera Giacomo, north of Concepción. Additionally at Concepción a biotite K-Ar age of 215±4 Ma (Triassic; Hervé *et al*., 1988) was indicated 85 km southwest of the city of Los Angeles and 70 km from the coastline at the Traiguén locality, a biotite K-Ar age of 298±4 Ma was published (Hervé *et al*., 1988). Furthermore, in the same area, the Nahuelbuta Mountains National Park, Hervé *et al*. (1988) obtained a biotite K-Ar age of 284±5 Ma. Glodny *et al*. (2008) present two-point Rb-Sr ages of 286.3±4.2 Ma (biotite-feldspar age) and 306.8±4.5 Ma (feldspar-muscovite age) on two intrusive igneous rocks of the same Nahuelbuta National Park region.

Initial $^{87}Sr/^{86}Sr$ ratios (ranging between 0.7057 and 0.7098) and εNd values (between -2 and -4) were obtained for granitoids and enclaves in the Santo Domingo Complex (Parada *et al*., 1999). Similar enriched isotopic compositions were determined for granitoids of *ca.* 294 Ma (Hervé *et al*., 1988) from Nahuelbuta with initial $^{87}Sr/^{86}Sr$ ratios varying in the range of 0.705 to 0.715 and εNd values in the range of -2.5 and -7.5 (Lucassen *et al*., 2004). These results indicate a mixing of at least two isotopically different lithospheric sources, with crust similar in composition to the exposed metasedimentary host rocks (Lucassen *et al*., 2004).

In the high Andes of Central Chile, Pineda and Calderón (2008) established through U-Pb zircon data a Carboniferous age of 328.1±2.8 Ma for a biotite-muscovite granite (Los Molles granite) and a Permian age of 294.2±2.3 Ma for a hornblende-biotite tonalite (El Pangue Tonalite), which belongs to the Elqui Limari Batholith (30-31ºS).

Willner *et al*. (2008) presented U-Pb zircon ages of 326±12 Ma and 294±4 Ma, Carboniferous and early Permian times, for two leucogranite pebble ages from the scarcely developed coastal accretionary prism between 31°-32°S. These authors indicate that initial εHf signatures on the same zircons range between +3.6 to -3.1, respectively. The crustal residence times are of 1.3-0.97 Ga, Meso- to Neoproterozoic, with slightly older model ages for the somewhat younger leucogranite samples. Furthermore, they suggest that Carboniferous samples are either the result of mixing of juvenile, mantle-derived magma with older crust or of recycling of crustal material distinct from the older magmatic products of the coastal accretionary system.

It is noteworthy that Martin *et al*. (1999b) dated late Paleozoic to Early Jurassic intrusive, volcanic and sedimentary rocks in the El Indio region close to the Argentinean border at 29-30°S. They interpreted their occurrence to be related to extensional processes that followed the cessation of Carboniferous to early Permian subduction along the western edge of Gondwana.

4. Analytical Procedures

4.1. SHRIMP U-Pb

Zircon grains were separated from whole rock samples using standard crushing, washing, heavy liquid (Sp. Gr. 2.96 and 3.3), and paramagnetic procedures. Hand selected zircon grains were placed onto double-sided tape, mounted in epoxy together with chips of the Temora reference zircon, sectioned approximately in half, and polished. Reflected and transmitted light photomicrographs were prepared for all zircons, as were cathodoluminescence (CL) Scanning Electron Microscope (SEM) images. These CL images were used to decipher the internal structures of the sectioned grains and to ensure that the ~20µm SHRIMP spot was wholly within a single age component within the sectioned grains.

The U-Th-Pb analyses were made using SHRIMP II at the Research School of Earth Sciences (RSES), The Australian National University, Canberra, Australia following procedures given in Williams (1998, and references therein). Each analysis consisted of 6 scans through the mass range, with Temora reference zircon grains analyzed for every three unknown analyses. The data have been reduced using the SQUID Excel Macro of Ludwig (2001). The Pb-U ratios have been normalised relative to a value of 0.0668 for the Temora reference zircon, equivalent to an age of 417 Ma (see Black *et al*., 2003). Uncertainty in the reference zircon calibration for each analytical session are given in the Table footnotes for each sample. Uncertainties given for individual analyses (ratios and ages) are at the one sigma level (Appendix 1). Tera & Wasserburg concordia plots, probability *versus* density plots with stacked histogram and weighted mean $^{206}Pb/^{238}U$ age calculations were carried out using ISOPLOT/EX (Ludwig, 2003). Weighted mean $^{206}Pb/^{238}U$ age calculation uncertainties are reported as 95% confidence limits. The geological time scale used is that of IUGS-ICS January 2013 (www.stratigraphy.org).

4.2. SHRIMP Oxygen

Oxygen isotope analyses were made using the RSES SHRIMP II fitted with a Cs source and electron gun for charge compensation following methods described by Ickert *et al*. (2008). The SHRIMP U-Pb analytical spots, craters approximately 20 μm in diameter by 1-2 μm deep were polished from the mount surface. The oxygen isotope analyses were then made on exactly the same location used for the U-Pb analyses. Oxygen isotope ratios were determined in multiple collector mode using an axial continuous electron multiplier (CEM) triplet collector, and two floating heads with interchangeable CEM - Faraday Cups. The Temora 2, Temora 3 and FC1 reference zircons were analysed to monitor and correct for isotope fractionation. The measured $^{18}O/^{16}O$ ratios and calculated $\delta^{18}O$ values have been normalised relative to an FC1 weighted mean $\delta^{18}O$ value of +5.4‰ (Ickert *et al*., 2008). Reproducibility in the Duluth Gabbro FC1 reference zircon $\delta^{18}O$ value ranged from ±0.266‰ to 0.509‰ (2σ uncertainty) for the analytical sessions. As a secondary reference, zircons from the Temora 2 and Temora 3 zircons analysed in the same analytical sessions gave $\delta^{18}O$ values of +8.2‰ and +7.59‰ respectively (2σ uncertainty), in agreement with data reported by Ickert *et al*. (2008) and unpublished data for the Temora 3 reference zircon.

4.3. LA-MC-ICPMS Lu-Hf

Lu-Hf isotopic measurements were conducted by laser ablation multicollector inductively coupled plasma mass spectroscopy (LA-MC-ICPMS) using the RSES Neptune MC-ICPMS coupled with a 193 nm ArF Excimer laser; similar to procedures described in Munizaga *et al*. (2008). Laser ablation analyses were performed on the same locations within single zircon grains used for both the U-Pb and oxygen isotope analyses. For all analyses of unknowns or secondary standards, the laser spot size was either ~47 μm or ~37 μm in diameter. The mass spectrometer was first tuned to optimal sensitivity using a large grain of zircon from the Mud Tank carbonatite. Isotopic masses were measured simultaneously in static-collection mode. A gas blank was acquired at regular intervals throughout the analytical session (every ≈10 analyses).

The laser was fired with typically 5-8 Hz repetition rate and 50-60 mJ energy. Data was acquired for 100 seconds, but in many cases only a selected interval from the total acquisition was used in data reduction. Throughout the analytical session several widely used reference zircons (91500, FC-1, Temora-2 and Mud Tank) were analysed to monitor data quality.

Signal intensity was typically *ca.* 5-6 V for total Hf at the beginning of ablation, and decreased over the acquisition time to 2 V or less. Isobaric interferences of ^{176}Lu and ^{176}Yb on the ^{176}Hf signal were corrected by monitoring signal intensities of ^{175}Lu and ^{173}Yb, ^{172}Yb and ^{171}Yb. The calculation of signal intensity for ^{176}Hf also involved independent mass bias corrections for Lu and Yb.

5. Results

5.1. Petrography

The nine studied samples are distributed within *ca.* 800 km distance along the Coastal Batholith, south-central Chile. Most important locality names referred to in the text are shown in figure 1. For exact localities and a summarized sample description refer to the corresponding Table 1.

The gneissic granodiorite (sample FO10-18), from the Playa Chica of the Quintay neighborhood, is composed of mainly plagioclase phenocrysts (35%), subordinately potassic feldspar (15%) and quartz (20%) with deformation lamellae that forms ribbons and subgrains (Hervé, 1976). Mafic minerals (30%) usually are biotite, hornblende and a variable amount of pyroxene. Some of these rocks contain hornblende with pyroxene inclusions. Abundant accessory minerals like zircon and apatite, subordinate amounts of titanite and epidote are present. This rock belongs to the Cochoa Unit of late Paleozoic age defined by Rivano *et al.* (1993).

The coarse-grained biotite-hornblende tonalite (sample FO10-99) from the Algarrobo locality is composed of quartz (30%), potassic feldspar (<3%) interstitial to plagioclase (34%), biotite (18%) in automorphic crystals and some with zircon and

TABLE 1. SUMMARIZED SAMPLE DESCRIPTION OF THE ANALYZED COASTAL BATHOLITH ROCKS.

Sample	Coordinates	Locality	Description
FO10-18	33°11’40.6”S 71°41’58.1”W	Playa Chica Quintay	Gneissic granodiorite with plagioclase phenocrystals, potassic feldspar and quartz; mafic minerals are hornblende, biotite and pyroxene; accessory minerals as zircon, apatite and some titanite and epidote.
FO10-99	33º21’47.7”S 71º41’12.2”W	Puntilla Algarrobo	Coarse grained biotite-hornblende tonalite with quartz and less potassic feldspar; accessory minerals are opaques, zircon, apatite and allanite.
FO10-08	34º18’40.1”S 71º44’17.1”W	Alcones Quarry	Biotite granite with cataclastic texture in all mineral constituents; main minerals are quartz, potassic feldspar, plagioclase; accessory minerals are titanite, allanite and zircon.
FO10-20	35º09’27.3 S 71º57’51.5”W	Llongocura	Coarse grained cataclastic biotite granite with large rounded quartz and microcline crystals, smaller plagioclase; slight sericitic or agillic alteration; apatite and zircon minerals.
FO09-59	36º31’30.5”S 72º57’13.7”W	Cullin Peninsula	Biotite quartz diorite with plagioclase; plagioclase minerals transformed to dark aggregates of fine grained epidote, chlorite and white mica; biotite shows alteration to chlorite and contains apatite and zircon inclusions.
FO09-54	37º40’13.4”S 73º07’11.2”W	Tres Pinos	Biotite granite with quartz, plagioclase, microcline and less hornblende; plagioclase shows epidote and white mica replacement; biotite contains some zircon and apatite inclusions.
FO09-53	37º41’30.5”S 73º08’31.5”W	Antihuala Nahuelbuta	Medium grained isotropic biotite hornblende granodiorite with quartz, potassic feldspar and plagioclase; biotite shows inclusions of zircon and apatite; some plagioclase crystals are saussuritized; accessory minerals are epidote and titanite.
FO09-38	40º19’20.5”S 72º21’30.5”W	Ilihue Lago Ranco	Medium grained biotite granodiorite with quartz, plagioclase and potassic feldspar; biotite is mostly and some amphiboles are chloritized; plagioclase is mostly sericitized.
FO09-205	33°10’11.8”S 71°41’7.5”W	Playa Grande Quintay	Quartz-bearing gabbro with hornblende. pyroxene plagioclase, quartz and titanite; accessory minerals are apatite, allanite and zircon.

apatite inclusions, and 15% of amphibole minerals. Amphibole occurs in automorphic poikilitic crystals including biotite, plagioclase and opaque minerals. Alteration minerals are chlorite in biotite, and epidote and white mica replacing plagioclase. Accessory minerals are opaques, zircon, apatite and allanite.

At Alcones, to the east of the Pichilemu coastal town, a biotite granite with cataclastic texture affecting all mineral constituents (sample FO10-08) was collected. The rock is composed of about 30% heavily deformed quartz with undulose texture and many sub-grains. Further on, the rock sample consists of 35% potassic feldspar in large crystals with poikilitic and many myrmekitic structures, 10% subidiomorphic plagioclase with deformed twin planes. Furthermore, the granite contains about 15% biotite mainly in deformed laths along micro-cataclastic bands. Accessory minerals are titanite, allanite and zircon.

A coarse grained cataclastic biotite granite sample (sample FO10-20) from Llongocura, 15 km to the east of Constitución, consists of large rounded quartz (35%) and the same amount of microcline crystals cut by tectonic microbreccias. Quartz is characterized by its undulose extinction. Microcline minerals often show myrmekite in the periphery. Plagioclase (25%) is present in smaller crystals frequently crushed in the microbreccias. Some minerals show sericitic or argillic alteration. Biotite flakes (5%) which occur in the microbreccias are altered to chlorite and prehnite. They frequently include apatite and zircon crystals.

The biotite quartz diorite (sample FO09-59) from the Punta Cullin locality, 60 km to the north of the city of Concepción, is mainly composed of 35% quartz and 40% plagioclase minerals, and some isolated biotite (25%) crystals. Primary plagioclase is mostly transformed to a dark aggregate, composed of very fine-grained epidote, chlorite and white mica. Biotite shows alteration to chlorite and has apatite and zircon inclusions.

The biotite granite (sample FO09-54) from the Tres Pinos locality in the Parque Nacional Nahuelbuta, is coarse-grained with an isotropic texture. It is composed of 30% quartz occurring as large rounded crystals with undulose extinction, 25% plagioclase laths with some crystals replaced by epidote and white mica, 25% interstitial microcline and 15% biotite which occurs in laths with zircon and apatite inclusions. Hornblende is less abundant (5%) and corroded, partially replaced by biotite.

At Antihuala, located in the Parque Nacional Nahuelbuta and about 30 km from the city of Angol, a medium-grained isotropic biotite hornblende granodiorite (sample FO09-53), is composed of 30% quartz, 25% microcline and 20% plagioclase. Biotite (15%) occurs in aggregates of smaller crystals. Amphibole (10%) appears in crystal clusters, some associated with biotite. Some biotite shows inclusions of zircon and apatite. Some plagioclase crystals are totally saussuritized. Accessory minerals are epidote and titanite.

From the southernmost locality of Ilihue, southern shore of the Lago Ranco and 70 km east of the town of La Unión, a medium grained isotropic biotite granodiorite (sample FO09-38) was collected. This belongs to the Principal Cordillera rather than the Coastal Range. It is composed of 30% quartz, 25% plagioclase, which is often included in big interstitial potassic feldspar (15%) in a monzonitic texture. Furthermore, biotite (20%) is mostly chloritized and contains occasionally titanite, prehnite and epidote. Amphibole (10%) is present in small euhedral prisms, with some chloritized rims. Plagioclase is mostly sericitized and encloses occasionally epidote and chlorite.

From the northernmost locality at the southern tip of Playa Grande at Quintay, sample FO09-205, belonging to the Laguna Verde Unit (Gana *et al*., 1996) of Jurassic age, is a quartz-bearing gabbro with hornblende and pyroxene. The sample is composed of 42% plagioclase (42%), quartz (3%), hornblende (45%), pyroxene (8%) and titanite (1%). Accessory minerals are apatite, allanite and zircon. Mafic and felsic bodies of this rock unit are intrusive into orthogneiss and granodiorites of Paleozoic age. South of Quintay town small lenses of metasedimentary rocks crop out, belonging to the Paleozoic Valparaíso Metamorphic complex. They comprise paragneissic bodies with hornstones and metaconglomerates (Hervé, 1976; Godoy and Loske, 1988).

5.2. Geochronology and Hf-O isotopes

The samples analyzed cover the north-south exposure of the Coastal Batholith between 33° and 40°S in south-central Chile (Fig. 1).

The gneissic granodiorite (FO10-18) yielded a weighted mean $^{206}Pb/^{238}U$ age of 311.5±3.3 Ma (95% confidence limits); the MSWD=1.4 for nineteen of twenty-one areas analyzed on 18 zircon grains (Figs. 2a, b). The initial $\varepsilon Hf_{(i)}$ values for FO10-18 are between -1.17 and -5.64. Two-stage Depleted Mantle model ages (T_{DM2}) range from 1.31 to 1.60 Ga indicating a significant crustal residence time with inferred separation from a Depleted Mantle source in the Mesoproterozoic. $\delta^{18}O$ ratios range from 6.61‰ to 7.30‰ with an average at 6.9‰ (Table 2; Appendixes 1a, 2a).

The coarse-grained tonalite with faint foliation (FO10-99) yielded an age of 308.9±2.4 Ma (2σ) with an MSWD of 1.2 for 19 of the 20 areas (Figs. 2c, d). The initial $\varepsilon Hf_{(i)}$ values record a relatively restricted range between -0.06 and -1.72. T_{DM2} range from 1.24 to 1.35 Ga implying crustal separation from the depleted mantle (DM) was likewise in Mesoproterozoic time. The $\delta^{18}O$ ratios are between 6.09 to 6.80‰, with an average of 6.4‰ for this sample (Table 2; Appendixes 1b, 2b).

The coarse grained biotite granite (FO10-08) has a calculated weighted mean age of 319.6±2.4 Ma (2σ) for 12 of the 22 analyzed zircon areas (Figs.

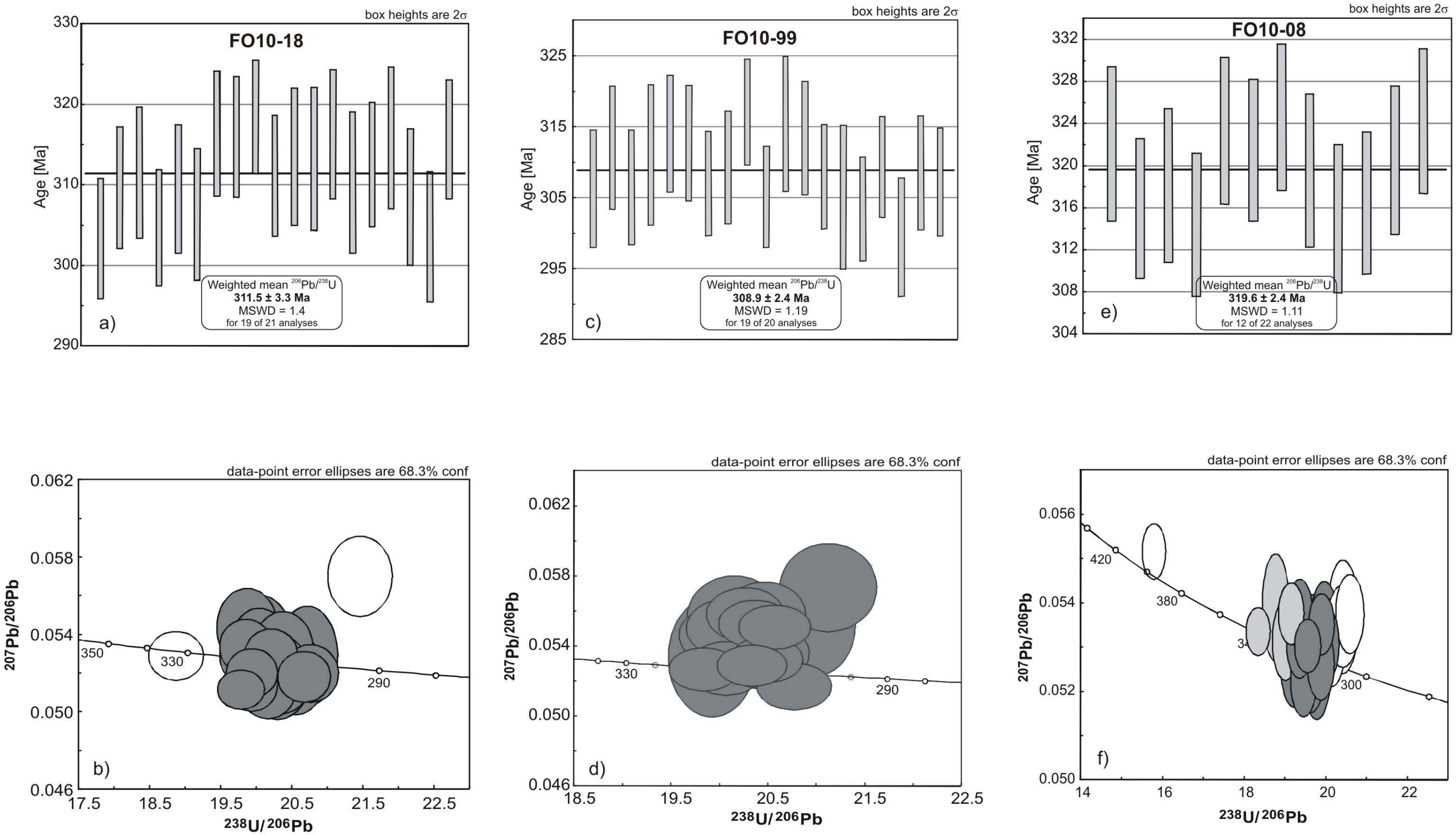

FIG. 2. Weighted mean age calculation and Tera & Wasserburg concordia plot for the U/Pb SHRIMP II data of **a+b)** gneissic granodiorite (sample FO10-18, Quintay); **c+d)** tonalite (sample FO10-99, Algarrobo) and **e+f)** biotite granite (sample FO10-08. Alcones), respectively.

TABLE 2. U/Pb SHRIMP II AGES, INITIAL εHf RATIOS AND δ18O VALUES OF THE COASTAL BATHOLITH SAMPLES.

Sample	Coordinates	Locality	Age (Ma)	$\varepsilon Hf_{(i)}$	$\delta^{18}O$ (%O) Range And Average
FO10-18	33°11'40.6"S 71°41'58.1"W	Playa Chica, Quintay	311.5±3.3 MSWD: 1.4	-1.17 to -5.64	6.61 to 7.30 ∅ 6.9
FO10-99	33º21'47.7"S 71º41'12.2"W	Puntilla Algarrobo	308.9±2.4 MSWD: 1.19	-0.06 to -1.72	6.09 to 6.80 ∅ 6.4
FO10-08	34º18'40.1"S 71º44'17.1"W	Alcones quarry	319.6±2.4 MSWD: 1.11	-1.11 to -3.56	6.32 to 7.84 (8.79 and 9.08) ∅ 7.3
FO10-20	35º09'27.3"S 71º57'51.5"W	Llongocura	300.8±2.4 MSWD: 0.99	+0.06 to -3.95	6.14 to 7.50 ∅ 6.6
FO09-59	36º31'30.5"S 72º57'13.7"W	Cullin peninsula	310.6±2.3 MSWD:1.3	-0.99 to -4.25	8.09 to 9.03 ∅ 8.6
FO09-54	37º40'13.4"S 73º07'11.2"W	Tres Pinos	309.2±2.2 MSWD: 1.5	+1.67 to -2.17	6.54 to 7.98 ∅ 7.4
FO09-53	37º41'30.5"S 73º08'31.5"W	Antihuala	310.2±2.5 MSWD: 1.3	+0.73 to -0.93	6.83 to 8.41 ∅ 7.7
FO09-38	40º19'20.5"S 72º21'30.5"W	Ilihue	305.9±2.4 MSWD: 0.98	+0.14 to -2.40	6.98 to 8.71 ∅ 7.7
FO09-205	33°10'11.8"S 71°41'7.5"W	Playa Quintay	168.9±1.4 MSWD: 1.04	+3.37 to +5.76	4.72 to 5.73 ∅ 5.3

2e, f). The calculated MSWD is 1.1 represented by 12 of 22 analyzed zircon areas. A secondary age group lies around 329.9±3.7 Ma (MSWD=0.74; n=4). Initial $\varepsilon Hf_{(i)}$ values are negative ranging from -1.11 to -3.56 with a Mesoproterozoic T_{DM2}. $\delta^{18}O$ ratios vary mainly between 6.32 and 7.84‰ with an average value of 7.3‰, excluding from the average calculation two outliers of 8.79 and 9.05‰ (Table 2; Appendixes 1c, 2c).

The coarse grained biotite-granite with potassic feldspar phenocrysts of up to 3 cm in length (FO10-20) yielded an age of 300.8±2.4 Ma with an MSWD of 0.99 for 19 of 20 analyzed grains (Figs. 3a, b). Sample FO10-20 shows an initial $\varepsilon Hf_{(i)}$ values between +0.06 and -3.95 and T_{DM2} ranging from 1.23 to 1.46 Ga. The average $\delta^{18}O$ ratio is 6.6‰ belonging to a range of 6.14 to 7.50‰ (Table 2, Appendixes 1d, 2d).

The intensely fractured fine-grained biotite granodiorite with dark inclusions (FO09-59) yielded an age of 310.6±2.3 Ma (MSWD=1.3 for 21 of 22 areas analyzed: Figs. 3c, d). The initial $\varepsilon Hf_{(i)}$ values range from -0.99 to -4.25 and yielded Mesoproterozoic T_{DM2} ages between 1.37 and 1.51 Ga. This granodiorite has the most elevated $\delta^{18}O$ ratio ranging from 8.09 to 9.03‰; average of 8.6‰ (Table 2; Appendixes 1e, 2e).

Sample FO09-54, a biotite granite gives an U-Pb SHRIMP age of 309.2±2.2 Ma with an MSWD of 1.5 for nineteen of twenty analyzed grains (Figs. 3e, f). The initial $\varepsilon Hf_{(i)}$ values are between +1.67 and -2.17 with slightly younger Mesoproterozoic T_{DM2} in the range 1.14 to 1.38 Ga. The $\delta^{18}O$ ratios are mostly between 6.54 to 7.98‰, with one higher at 8.82‰; the overall mean value is 7.4‰ (Table 2; Appendixes 1f, 2f).

The biotite granite (FO09-53) yielded an U-Pb age of 310.2±2.5 Ma (2σ) with a MSWD of 1.3 calculated for 19 of 21 analyzed zircon areas (Figs. 4a, b). Sample FO09-53 indicates a narrow range of initial $\varepsilon Hf_{(i)}$ values from +0.73 to -0.93. The calculated crustal residence time is the same as shown by the other sample sites indicating Mesoproterozoic T_{DM2} between 1.19 to 1.32 Ga. The $\delta^{18}O$ ratio shows an average of 7.7‰ on all analyzed zircon crystals; the range is from 6.83 to 8.41‰ (Table 2; Appendixes 1g, 2g).

The biotite-amphibole granodiorite (FO09-38) yielded an age of 305.9±2.4 Ma with a MSWD of 0.98 from 22 over 24 areas analyzed (Figs. 4c, d). The initial $\varepsilon Hf_{(i)}$ ranges from +0.14 to -2.40. The calculated T_{DM2} record a similar Mesoproterozoic range (1.23 to 1.39 Ga) as seen in the other sample sites and, the overall mean $\delta^{18}O$ ratio of 7.7‰ with a range from 6.98 to 8.71‰ (Table 2; Appendixes 1h, 2h).

The northernmost analyzed sample, a hornblende-pyroxene quartz-gabbro (FO09-205) contributed with an unexpected Middle Jurassic age 168.9±1.1 Ma for 18 selected spots (Fig. 4e, f; MSWD=1.04). The $\delta^{18}O$ ratios range from 4.72 to 5.73‰ with an average of 5.3‰ equivalent to mantle value of 5.3‰ The initial $\varepsilon Hf_{(i)}$ values range between +3.37 and +5.76. Crustal T_{DM2} values are indicating Neoproterozoic residences times (Table 2; Appendixes 1i, 2i).

In summary, the eight Paleozoic granitoid samples corresponding to a north-to-south distance along the Coastal Batholith of *ca.* 800 km record a narrow range in crystallization ages between 300.8±2.4 Ma and 319.6±2.4 Ma, Pennsylvanian (late Carboniferous), with five of the granitoids within uncertainty at ~309 Ma (Fig. 5). The initial Hf-isotopic composition, $\varepsilon Hf_{(i)}$ on the dated zoned igneous zircon areas range from +1.67 to -5.64 (Fig. 6a), but the majority of the analyses are between a more restricted range of +1 to -4 epsilon units. The T_{DM2} all suggest Mesoproterozoic crustal residence ages, but with some subtle variations. The $\delta^{18}O$ average ratios range from 6.4 to 8.6‰ for the Pennsylvanian samples (Fig. 6b) and in detail there is a more prominent group between 6.0 to 7.5‰ with a lesser group at 8.0 to 9.0‰. The observed minor data discrepancy within each isotope system does not validate any time-space tendency. Additionally, this data clearly shows that the magmas are derived from crustal sources, that is, those that have had a prominent sedimentary input in order to achieve the elevated $\delta^{18}O$ values. However one cannot preclude the total absence of a mantle input. Together, the O and Hf data are in agreement with likely magmatic sources being older crustal components (Mesoproterozoic T_{DM2}), enriched in sedimentary components (elevated $\delta^{18}O$).

The Middle Jurassic sample from the northernmost sample site provides a clear difference to the older intrusives: inferred crustal residence time is Neoproterozoic, initial $\varepsilon Hf_{(i)}$ values are positive between +3.4 to +5.8 and $\delta^{18}O$ average indicates a mantle value of 5.3‰.

6. Discussion and Conclusions

On the basis of our new data, the Pennsylvanian Coastal Batholith in south-central Chile is shown to have been emplaced in a very short period of time (20 Ma) and to be relatively homogeneous in crystallization age and both Hf and O isotopic compositions along 800 km length, regardless of rock types which vary from quartz diorite to granite. After a 150 Ma magmatic lull, Jurassic quartziferous gabbros of much more primitive isotopic composition were emplaced through the Paleozoic rocks of the Coastal Batholith in the northern study area. This evolution is very different to what is observed in the Mesozoic to Cenozoic batholiths in northern Chile (Dallmeyer *et al.*, 1996) and in the South Patagonian batholith (Hervé *et al.*, 2007b) which are typical Andean batholiths, the last with large age range -spanning from 155 to 5 Ma- and greater variation in Hf and O isotopic compositions (Fanning *et al.*, 2010).

This suggests a relative homogeneous source with a significant continental crust component for these magmas. The two stage Depleted Mantle model age calculations all yield Mesoproterozoic ages which indicate that the source(s) for the magmas from which the zircon crystallized have had a significant residence time in the crust. If this was the case, then the magmatic arc would have been formed on continental crust ($\delta^{18}O$ >5.3±0.6; Fig. 6), beyond the backstop of the accretionary complex to the west. This suggests that the Eastern Series, which the batholiths intrudes, was deposited over this continental crust or either has been tectonically transported from the west to its present position over the western edge of continental crust. Alternatively, part or all of the melting crustal material could correspond to sediments transported deep into mantle wedge by the subducted crust, as modeled by Gerya and Meilick (2011). The fast extinction of the arc, which appears to have lasted less than 20 Ma, was probably the consequence of changes in the subduction parameters, which displaced the melting conditions of the underlying crust from the site of the Coastal Batholith to the east. These changes could be related with the contraction of the Rheic Ocean that culminated with the collision of NW Gondwana and south-eastern Laurentia at *ca.* 320 Ma (McElhinny *et al.*, 2003). It is interesting to consider that during the span in which the south-central Coastal Batolith was emplaced Gondwana

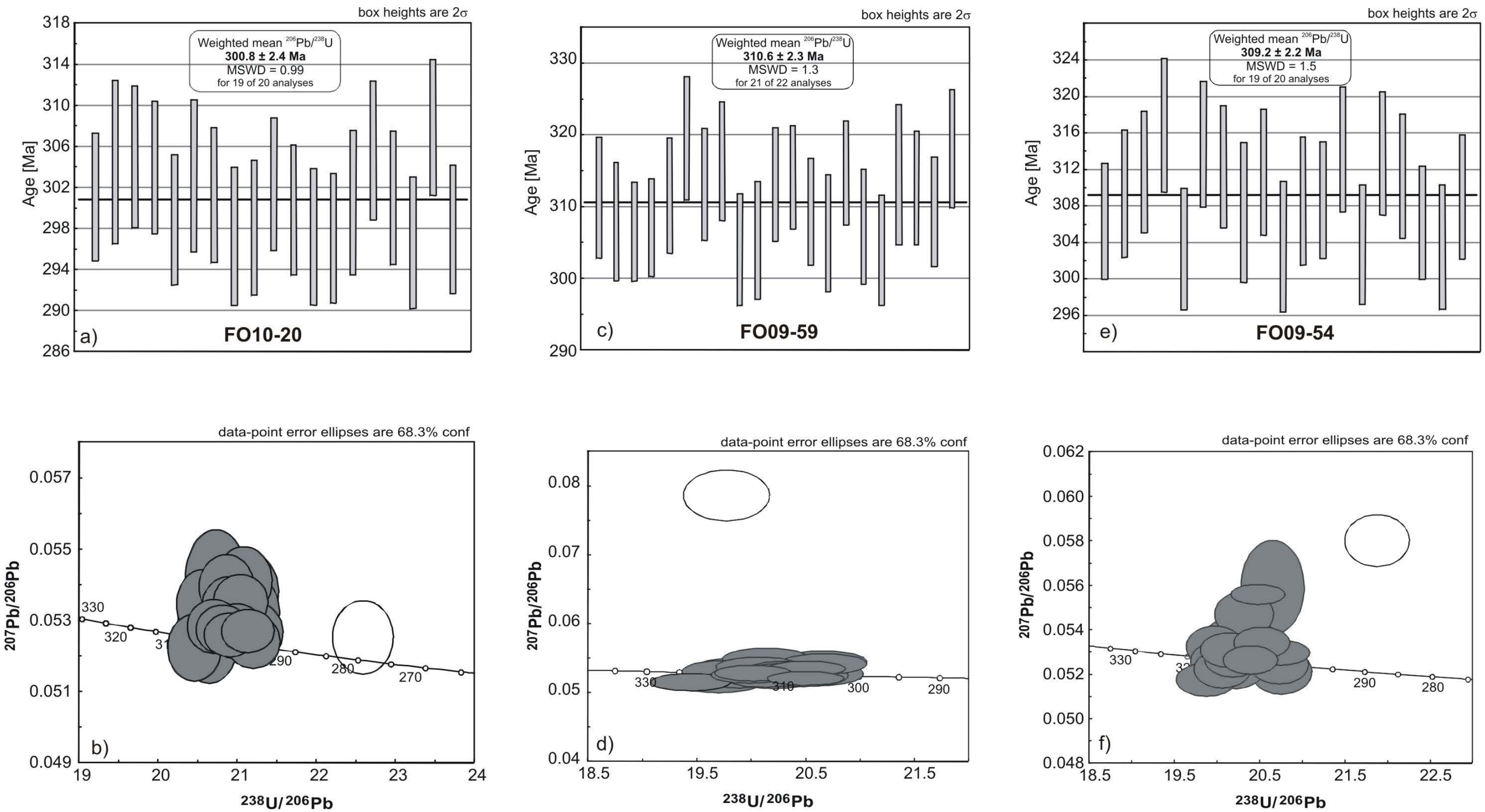

FIG. 3. Weighted mean age calculation and Tera & Wasserburg concordia plot of U-Pb SHRIMP II data of **a+b**) biotite granite (sample FO10-20. Llongocura); **c+d**) biotite quartz diorite (sample FO09-59, Cullín) and **e+f**) biotite granite (sample FO09-54, Tres Pinos), respectively.

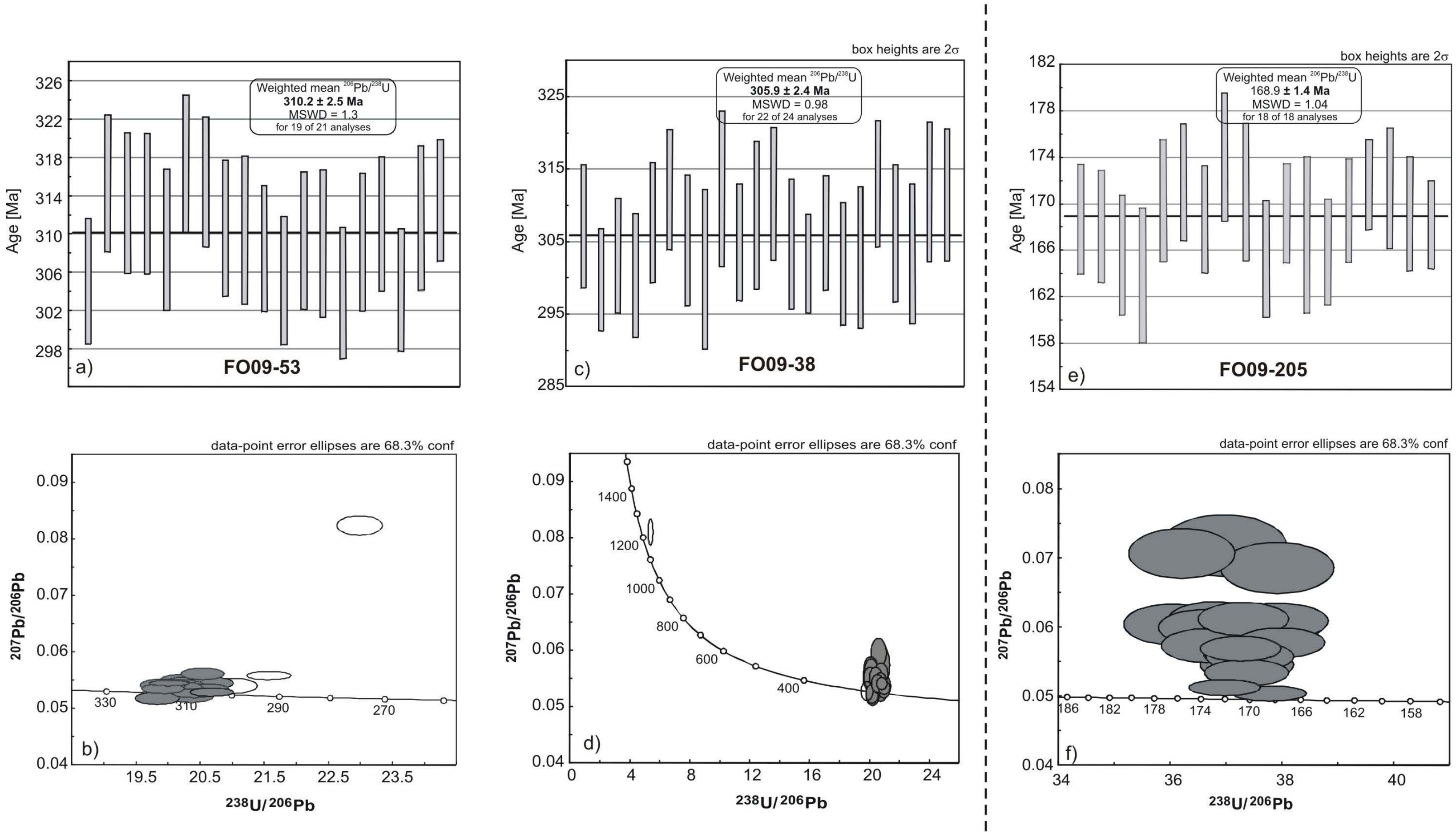

FIG. 4. Weighted mean age calculation and Tera & Wasserburg Concordia plot of U-Pb SHRIMP II data of **a+b)** biotite granite, (sample FO09-53, Antihuala); **c+d)** hornblende-biotite granitodiorite (sample FO09-38. Lilhue) and **e+f)** quartziferous gabbro (sample FO09-205. Quintay), respectively.

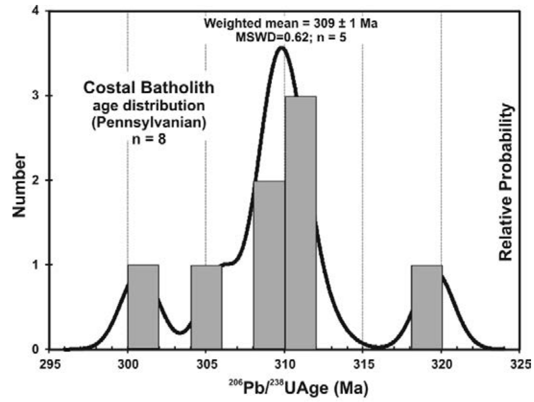

FIG. 5. Age probability plot for the Late Carboniferous Coastal Batholith granite to diorite samples between 30° and 40°S, Chile.

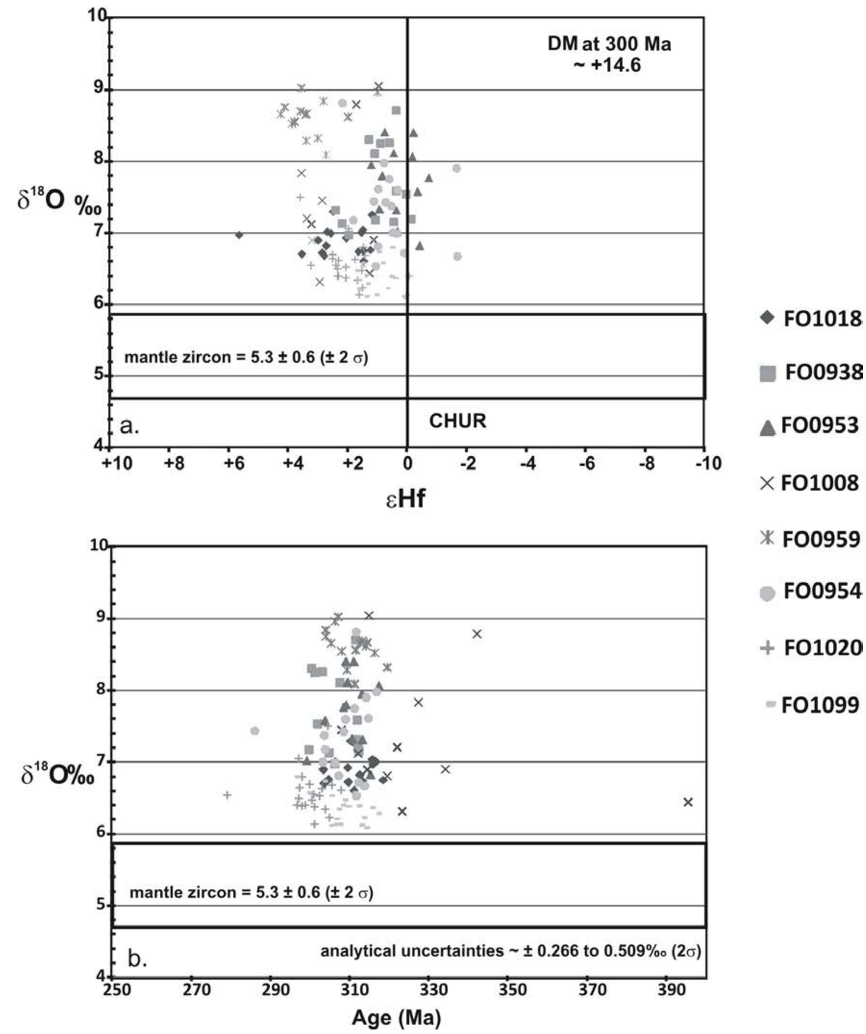

FIG. 6. **a.** Initial εHf *versus* $\delta^{18}O$ diagram; **b.** Age (Ma) *versus* $\delta^{18}O$ diagram.

remained in a relative stationary position (Oviedo and Vilas, 1984) in contrast with fast movements and rotations before and after that time (Geuna *et al*., 2010).

The Coastal Batholith was eroded to a similar level as the present one, before deposition of the Late Triassic (Norian) sedimentary rocks (Nielsen, 2005). Surprisingly, detrital zircon derived from the batholith are not found as constituents of the Permian accretionary prism which constitute the Western Series south of 38°S (Hervé *et al*., 2013), a probable indication that significant portions of the accretionary complex do not crop out. It is interesting to note that the evolution of the accretionary prism continued until the Triassic, when Late Triassic plutonic bodies beside some locally restricted post-subduction A-type granitoids intruded into the Western Series (Vásquez and Franz, 2008).

Acknowledgements

This work was financed through the Chilean Grant FONDECYT 1095099.

We would like to thank J. Vargas and R.Valles at the Geology Department, Universidad de Chile, for the zircon separation. M. Solari and M. Vásquez accompanied some of the field trips. A. González, P. Castillo, E. Salazar, and F. Poblete helped taking difficult samples in the northern section of the Coastal Batholith. Thorough revisions by C. Casquet (Universidad de Madrid) and F. Lucassen (University of Bremen) greatly improved the original manuscript.

References

Aguirre, L.; Hervé, F.; Godoy, E. 1972. Distribution of metamorphic facies in Chile, an outline. Kristalinikum 9: 7-19.

Bouvier, A.; Vervoort, J.D.; Patchett, P.J. 2008. The Lu-Hf and Sm-Nd isotopic composition of CHUR: Constraints from unequilibrated chondrites and implications for the bulk composition of terrestrial planets. Earth and Planetary Science Letters 273: 48-57.

Barazangi, M.; Isacks, B.L. 1976. Spatial distribution of earthquakes and subduction of the Nazca plate beneath South America. Geology 4: 686-692.

Black, L.P.; Kamo, S.L.; Allen, C.M.; Aleinikoff, J.N.; Davis, D.W.; Korsch, R.J.; Foudoulis, C. 2003. TEMORA 1: A new zircon standard for Phanerozoic U-Pb geochronology. Chemical Geology 200: 155-170.

Cahill, T.; Isacks, B.L. 1992. Seismicity and shape of the subducted Nazca plate. Journal of Geophysical Research 97: 17503-17529.

Cordani, U.; Munizaga, F.; Hervé, F.; Hervé, M. 1976. Edades radiométricas provenientes del basamento cristalino de la Cordillera de la Costa de las provincias de Valparaíso y Santiago, Chile. *In* Congreso Geológico Chileno, No. 1, Actas 2: F213-F221. Santiago.

Dallmeyer, R.D.; Brown, M.; Grocott, J.; Taylor, G.K.; Treloar, P.J. 1996. Mesozoic Magmatic and Tectonic Events within the Andean Plate Boundary Zone, 26°-27°30'S, North Chile: Constraints from Mineral Ages. The Journal of Geology 104 (1): 19-40.

Duhart, P.; McDonough, M.; Muñoz, J.; Martin, M.; Villeneuve, M. 2001. El Complejo Metamórfico Bahía Mansa en la cordillera de la Costa del centro-sur de Chile (39°30'-42°00'S): geocronología K-Ar, $^{40}Ar/^{39}Ar$ y U-Pb e implicancias en la evolución del margen sur-occidental de Gondwana. Revista Geológica de Chile 28 (2): 179-208.

Fanning, C.M.; Hervé, F.; Pankhurst, R.J.; Calderón, M.; Yaxley, G.; Holden, P. 2010. Zircon oxygen and Hf isotopic constraints on 150 m.y. of subduction magmatism, South Patagonian Batholith, South America. Geochimica et Cosmochimica Acta 74 (12): A279-A279.

Gana, P.; Tosdal, R. 1996. Geocronología U-Pb y K-Ar en intrusivos del Paleozoico y Mesozoico de la Cordillera de la Costa, Región de Valparaíso, Chile. Revista Geológica de Chile 23 (2): 151-164.

Gana, P.; Wall, R.; Gutiérrez, A. 1996. Mapa geológico del área de Valparaíso-Curacaví, regiones de Valparaíso y Metropolitana. Servicio Nacional de Geología y Minería. Chile, Mapas Geológicos 1, mapa 1:100.000.

Gerya, T.V.; Meilick, F.I. 2011. Geodynamic regimes of subduction under an active margin: effects of rheological weakening by fluids and melts. Journal of Metamorphic Geology 29: 7-31.

Geuna, S.E.; Escosteguy, L.D.; Limarino, C.O. 2010. Paleomagnetism of the Carboniferous-Permian Patquía Formation, Paganzo basin, Argentina: implications for the apparent polar wander path for South America and Gondwana during the Late Paleozoic. Geologica Acta 8 (4): 373-397.

Glodny, J.; Echler, H.; Collao, S.; Ardiles, M.; Buron, P.; Figueroa, O. 2008 Differential Late Paleozoic active margin evolution in South-Central Chile (37º-40ºS)-the Lanalhue Fault Zone. Journal of South American Earth Sciences 26: 397-411.

Godoy, E. 1970. El granito de Constitución y su aureola metamórfica. Memoria de Título (Unpublished), Departamento de Geología, Universidad de Chile: 144 p.

Godoy, E.; Loske, W. 1988. Tectonismo sinplutónico de dioritas jurásicas al sur de Valparaíso: datos U-Pb sobre la 'Fase Quintay'. Revista Geológica de Chile 15 (2): 119-127.

Goodge, J.W.; Vervoort, J.D. 2006. Origin of Mesoproterozoic A-type granites in Laurentia: Hf isotope evidence. Earth and Planetary Science Letters 243: 711-731.

Hager, B.H.; O'Connell, R.J. 1978. Subduction zone dip angles and flow driven by plate motion. Tectonophysics 50: 111-133.

Hernández, L. 2006. Rocas Máficas y Ultramáficas en Laguna Verde, Chile Central. Graduation Thesis (Unpublished), Universidad de Chile: 155 p.

Hervé, F. 1976. Petrografía del Basamento Cristalino en el área Laguna Verde-Quintay, Provincia de Valparaíso, Chile. *In* Congreso Geológico Chileno No. 1, Actas 2: F-125-F-143. Santiago.

Hervé, F. 1977. Petrology of the crystalline basement of the Nahuelbuta mountains, south central Chile. *In* Comparative studies on the geology of the Circum-Pacific orogenic belt in Japan and Chile. *In* Japanese Society for the Promotion of Sciences (Ishikawa, T.; Aguirre, L.; editors): 1-51.

Hervé, F.; Munizaga, F.; Parada, M.A.; Brook, M.; Pankhurst, R.J.; Snelling, N.J.; Drake, R. 1988. Granitoids of the Coast Range of Central Chile: Geochronology and geologic setting. Journal of South American Earth Sciences 1 (2): 185-194.

Hervé, F.; Faúndez, V.; Calderón, M.; Massonne, H.-J.; Willner, A.P. 2007a. Metamorphic and plutonic basement complexes. *In* The Geology of Chile (Moreno, T.; Gibbons, W.; Ishikawa, T.; Aguirre, L.; editors). Geological Society, Special Volume: 5-19. London.

Hervé, F.; Pankhurst, R.J.; Fanning, C.M.; Calderón, M.; Yaxley, G.M. 2007b. The South Patagonian batholith: 150 my of granite magmatism on a plate margin. Lithos 97: 373-394.

Hervé, F.; Calderón, M.; Fanning, C.M.; Pankhurst, R.J.; Godoy, E. 2013. Provenance variations in the Late Paleozoic accretionary complex of central Chile as indicated by detrital zircons. Gondwana Research 23: 1122-1135

Ickert, R.B.; Hiess, J.; Williams, I.S.; Holden, P.; Ireland, T.R.; Lanc, P.; Schram, N.; Foster, J.J.; Clement, S.W. 2008. Determining high precision, in situ, oxygen isotope ratios with a SHRIMP II: Analyses of MPI-DING silicate-glass reference materials and zircon from contrasting granites. Chemical Geology 257: 114-128.

Jordan, T.E.; Isacks, B.L.; Allmendinger, R.W.; Brewer, J.A.; Ramos, V.A.; Ando, C.J. 1983. Andean tectonics related to the geometry of subducted Nazca plate. Geological Society American Bulletin 94: 341-361.

Lucassen, F.; Trumbull, R.; Franz, G.; Creixell, C.; Vásquez, P.; Romer, R.L.; Figueroa, O. 2004. Distinguishing crustal recycling and juvenile additions at active continental margins: the Paleozoic to Recent compositional evolution of the Chilean Pacific margin (36-41°S). Journal of South American Earth Sciences 17: 103-119.

Ludwig, K.R. 2001. SQUID 1.02, A User's Manual; Berkeley Geochronology Center Special Publication. No. 2, 2455 Ridge Road, Berkeley, CA 94709, USA.

Ludwig, K.R. 2003. User's manual for Isoplot/Ex, Version 3.0, A geochronological toolkit for Microsoft Excel. Berkeley Geochronology Center Special Publication No. 4, 2455 Ridge Road, Berkeley CA 94709, USA.

Martin, M.W.; Kato, T.T.; Rodríguez, C.; Godoy, E.; Duhart, P.; McDonough, M.; Campos, A. 1999a. Evolution of the late Paleozoic accretionary complex and overlying forearc-magmatic arc, south central Chile (38°-41°S): constraints for the tectonic setting along the southwestern margin of Gondwana. Tectonics 18: 582-605.

Martin, M.W.; Clavero, J.; Mpodozis, C. 1999b. Late Palaeozoic to Early Jurassic tectonic development of the high Andean Principal Cordillera, El Indio region, Chile (29º-30ºS). Journal of South American Earth Sciences 12: 33-49.

McElhinny, M.W.; Powell, Ch.McA.; Pisarevsky, S.A. 2003. Paleozoic terranes of eastern Australia and the drift history of Gondwana. Tectonophysics 362: 41-65.

Munizaga, F.; Maksaev, V.; Fanning, C.M.; Giglio, S.; Yaxley, G.; Tassinari, C.C.G. 2008. Late Paleozoic-Early Triassic magmatism on the western margin of Gondwana: Collahuasi area, Northern Chile. Gondwana Research 13: 407-427.

Nielsen, S. 2005. The Triassic Santa Juana Formation at the lower Biobío River, south central Chile. Journal of South American Earth Sciences 19: 547-562.

Oviedo, E.S.; Vilas, J.F.A. 1984. Movimientos recurrentes en el Permo-Triásico entre Gondwana Occidental y el Oriental. San Carlos de Bariloche. *In* Congreso Geológico Argentino, No. 9, Actas 3: 97-114. San Carlos de Bariloche.

Parada, M.A.; Levi, B.; Nyström, J.O. 1991. Geochemistry of the Triassic to Jurassic plutonism of Central Chile (30 to 33°S); petrogenetic implications and a tectonic discussion. *In* Andean Magmatism and its Tectonic Setting (Harmon, R.S.; Rapela, C.W.; editors). Geological Society of America, Special Papers 265: 99-112. Boulder, Colorado.

Parada, M.A.; Nyström, J.O.; Levi, B. 1999. Multiple sources for the Coastal Batholith of central Chile (31-34°S): geochemical and Sr-Nd isotopic evidence and tectonic implications. Lithos 46: 505-521.

Parada, M.A.; López-Escobar, L.; Oliveros, V.; Fuentes, F.; Morata, D.; Calderón, M.; Aguirre, L.; Féraud, G.; Espinoza, F.; Moreno, H.; Figueroa, O.; Muñoz Ravo, J.; Troncoso Vásquez, R.; Stern, C.R. 2007. Andean Magmatism. *In* 'The Geology of Chile' (Moreno, T.; Gibson, W.; editors). The Geological Society, London, Special Publication 4: 115-146.

Pineda, G.; Calderón, M. 2008. Geología del área Monte Patria-El Maqui, Región de Coquimbo. Servicio Nacional de Geología y Minería, Carta Geológica de Chile, Serie Geología Básica 116: 44 p., 1 mapa escala 1:100.000.

Ramírez, V. 2010. Plutonismo del carbonífero superior y jurásico medio en el tramo costero entre Laguna Verde y Tunquén (33°05'-33°15'S), Chile central. Graduation Thesis (Unpublished), Universidad de Chile: 122 p.

Rapela, C.W.; Pankhurst, R.J.; Fanning, C.M.; Grecco, L.E. 2003. Basement evolution of the Sierra de la Ventana Fold Belt: new evidence for Cambrian continental rifting along the southern margin of Gondwana. Journal of the Geological Society of London 160: 613-628. London.

Rivano, S.; Sepúlveda, P.; Boric, P.; Espiñeira, D. 1993. Hojas Quillota y Portillo, V Región. Servicio Nacional de Geología y Minería, Carta Geológica de Chile 73, 1 mapa escala 1:250.000. Acompaña Informe Inédito 7644.

SERNAGEOMIN, 2003. Mapa Geológico de Chile: version digital. Gobierno de Chile, Servicio Nacional de Geología y Minería, Subdirección Nacional de Geología, Publicación Geológica Digital 4, CD-ROM, versión 1.0. Base Geológica escala 1:1.000.000.

Shibata, K.; Ishihara, S.; Ulriksen, C. 1984. Rb-Sr ages and initial $^{87}Sr/^{86}Sr$ ratios of late Paleozoic granitic rocks from northern Chile. Bulletin of the Geological Survey of Japan 35 (2): 537-545.

Söderlund, U.; Patchett, P.J.; Vervoort, J.D.; Isachsen, C.E. 2004. The 176Lu decay constant determined by Lu-Hf and U-Pb isotope systematics of Precambrian mafic intrusions. Earth and Planetary Science Letters 219: 311-324.

Tera, F.; Wasserburg, G. 1972. U-Th-Pb systematics in three Apollo 14 basalts and the problem of initial Pb in lunar rocks. Earth and Planetary Science Letters 14: 281-304.

Vásquez, P.; Franz, G. 2008. The Triassic Cobquecura Pluton (Central Chile): An example of a fayalite-bearing A-type intrusive massif at a continental margin. Tectonophysics 459: 66-84.

Vervoort, J.D.; Blichert-Toft, J. 1999. Evolution of the depleted mantle: Hf isotope evidence from juvenile rocks through time. Geochimica et Cosmochimica Acta 63: 533-556.

Wall, R.; Gana, P.; Gutiérrez, A. 1996. Geología de la Hoja Santiago, área de San Antonio-Melipilla, regiones de Valparaíso, Metropolitana y del Libertador General Bernardo O'Higgins. Servicio Nacional de Geología y Minería, Mapas Geológicos 2, 1 mapa escala 1:100.000, anexo.

Williams, I.S. 1998. U-Th-Pb Geochronology by Ion Microprobe. *In* Applications of microanalytical techniques to understanding mineralizing processes (McKibben, M.A.; Shanks III, W.C.; Ridley, W.I.; editors). Reviews in Economic Geology 7: 1-35.

Willner, A.P.; Thomson, S.N.; Kröner, A.; Wartho, J.-A.; Wijbrans, J.R.; Hervé, F. 2005. Time Markers for the Evolution and Exhumation History of a Late Palaeozoic Paired Metamorphic Belt in North-Central Chile (34°-35°3'S). Journal of Petrology 46 (9): 1835-1858.

Willner, A.P.; Gerdes, A.; Massonne, H.-J. 2008. History of crustal growth and recycling at the Pacific convergent margin of South America at latitudes 29°-36°S revealed by a U-Pb and Lu-Hf isotope study of detrital zircon from late Paleozoic accretionary systems. Chemical Geology 253 (3-4): 114-129.

Manuscript received: October 12, 2012; revised/accepted: May 2, 2013; available online: May 2, 2013.

APPENDIX 1a. SUMMARY OF SHRIMP U-Pb RESULTS FOR ZIRCON FROM SAMPLE FO10-18, QUINTAY.

							Total				Radiogenic		Age (Ma)	
Grain. spot	**U (ppm)**	**Th (ppm)**	**Th/U**	**$^{206}Pb^*$ (ppm)**	**$^{204}Pb/^{206}Pb$**	**f_{206} %**	**$^{238}U/^{206}Pb$**	**±**	**$^{207}Pb/^{206}Pb$**	**±**	**$^{206}Pb/^{238}U$**	**±**	**$^{206}Pb/^{238}U$**	**±**
1.1	259	105	0.41	10.7	-	<0.01	20.76	0.26	0.0520	0.0010	0.0482	0.0006	303.4	3.7
2.1	273	124	0.46	11.5	0.000436	<0.01	20.35	0.25	0.0514	0.0010	0.0492	0.0006	309.7	3.8
3.1	203	131	0.64	8.7	0.000316	<0.01	20.20	0.27	0.0525	0.0011	0.0495	0.0007	311.6	4.1
4.1	336	243	0.72	14.0	0.000378	<0.01	20.67	0.25	0.0518	0.0009	0.0484	0.0006	304.7	3.6
5.1	216	77	0.36	9.1	-	<0.01	20.34	0.26	0.0523	0.0011	0.0492	0.0006	309.6	4.0
6.1	183	80	0.44	7.7	0.001003	<0.01	20.56	0.28	0.0519	0.0014	0.0487	0.0007	306.4	4.1
7.1	286	127	0.44	12.4	0.000364	0.08	19.86	0.25	0.0534	0.0009	0.0503	0.0006	316.5	3.9
7.2	322	133	0.41	13.9	0.000080	<0.01	19.94	0.24	0.0514	0.0009	0.0502	0.0006	316.0	3.8
8.1	539	79	0.15	23.4	-	<0.01	19.78	0.22	0.0512	0.0007	0.0506	0.0006	318.5	3.5
9.1	298	129	0.43	12.7	-	0.04	20.21	0.25	0.0529	0.0009	0.0495	0.0006	311.2	3.8
10.1	164	77	0.47	7.0	-	0.10	20.04	0.28	0.0534	0.0013	0.0498	0.0007	313.6	4.3
11.1	140	45	0.32	6.0	0.000801	0.16	20.05	0.29	0.0539	0.0014	0.0498	0.0007	313.3	4.4
12.1	243	123	0.51	10.5	-	0.03	19.88	0.25	0.0529	0.0010	0.0503	0.0007	316.3	4.0
12.2	374	56	0.15	17.0	0.000075	<0.01	18.87	0.26	0.0529	0.0008	0.0530	0.0007	332.9	4.5
13.1	169	61	0.36	6.8	0.001103	0.61	21.45	0.30	0.0570	0.0014	0.0463	0.0007	291.9	4.1
14.1	159	59	0.37	6.7	-	<0.01	20.30	0.29	0.0516	0.0013	0.0493	0.0007	310.3	4.4
15.1	298	135	0.45	12.7	0.000253	<0.01	20.16	0.25	0.0511	0.0010	0.0497	0.0006	312.6	3.9
16.1	152	94	0.62	6.6	0.000643	0.21	19.87	0.28	0.0544	0.0013	0.0502	0.0007	315.9	4.4
16.2	177	78	0.44	7.5	0.000104	0.10	20.38	0.28	0.0533	0.0013	0.0490	0.0007	308.5	4.2
17.1	199	85	0.43	8.2	-	0.06	20.72	0.28	0.0529	0.0017	0.0482	0.0007	303.6	4.1
18.1	389	139	0.36	16.7	0.000149	<0.01	19.94	0.24	0.0520	0.0008	0.0502	0.0006	315.7	3.7

Notes:

1. Uncertainties given at the one σ level.
2. Error in Temora reference zircon calibration was 0.75% for the analytical session (not included in above errors but required when comparing data from different mounts).
3. f_{206} % denotes the percentage of ^{206}Pb that is common Pb.
4. Correction for common Pb for the U-Pb data has been made using the measured $^{238}U/^{206}Pb$ and $^{207}Pb/^{206}Pb$ ratios following Tera and Wasserburg (1972) as outlined in Williams (1998).

APPENDIX 1b. SUMMARY OF SHRIMP U-Pb RESULTS FOR ZIRCON FROM SAMPLE FO10-99, TONALITE, ALGARROBO.

							Total				Radiogenic		Age (Ma)	
Grain. spot	U (ppm)	Th (ppm)	Th/U	^{206}Pb* (ppm)	^{204}Pb/ ^{206}Pb	f_{206} %	^{238}U/ ^{206}Pb	±	^{207}Pb/ ^{206}Pb	±	^{206}Pb/ ^{238}U	±	^{206}Pb/ ^{238}U	±
1.1	120	53	0.44	5.0	0.000231	0.41	20.47	0.28	0.0558	0.0012	0.0487	0.0007	306.3	4.2
2.1	106	30	0.28	4.5	0.000968	0.25	20.11	0.28	0.0546	0.0013	0.0496	0.0007	312.1	4.4
3.1	140	67	0.48	5.9	0.000336	0.14	20.51	0.27	0.0536	0.0011	0.0487	0.0007	306.5	4.0
4.1	66	37	0.56	2.8	0.001837	0.38	20.15	0.32	0.0556	0.0016	0.0494	0.0008	311.0	4.9
5.1	139	59	0.42	6.0	0.000277	0.24	19.98	0.26	0.0546	0.0011	0.0499	0.0007	314.0	4.1
6.1	145	68	0.47	6.2	0.000625	0.30	20.06	0.26	0.0550	0.0011	0.0497	0.0007	312.7	4.1
7.1	217	150	0.69	9.1	0.000568	0.09	20.48	0.25	0.0532	0.0009	0.0488	0.0006	307.0	3.7
8.1	207	143	0.69	8.8	0.000683	0.40	20.26	0.26	0.0558	0.0010	0.0492	0.0006	309.3	4.0
9.1	249	115	0.46	10.8	0.000161	<0.01	19.84	0.24	0.0527	0.0008	0.0504	0.0006	317.1	3.7
10.1	254	161	0.64	10.6	0.000239	0.33	20.57	0.25	0.0551	0.0008	0.0485	0.0006	305.1	3.6
11.1	82	42	0.51	3.5	0.001000	0.08	19.92	0.30	0.0534	0.0022	0.0502	0.0008	315.5	4.7
12.1	159	65	0.41	6.8	0.000260	0.01	20.07	0.26	0.0527	0.0010	0.0498	0.0006	313.4	4.0
13.1	222	146	0.66	9.4	0.000448	0.34	20.37	0.25	0.0553	0.0009	0.0489	0.0006	308.0	3.7
14.1	80	51	0.64	3.3	0.001317	0.64	21.12	0.33	0.0573	0.0017	0.0470	0.0008	296.3	4.6
15.1	59	18	0.31	2.4	0.000235	0.29	20.57	0.34	0.0548	0.0017	0.0485	0.0008	305.1	5.1
16.1	210	144	0.69	8.7	0.000242	<0.01	20.77	0.25	0.0517	0.0009	0.0482	0.0006	303.4	3.7
17.1	284	146	0.51	12.0	0.000300	0.04	20.33	0.24	0.0529	0.0008	0.0492	0.0006	309.3	3.6
18.1	110	38	0.35	4.5	0.001130	0.34	20.96	0.29	0.0551	0.0019	0.0476	0.0007	299.5	4.2
19.1	143	97	0.68	6.0	0.000484	0.09	20.38	0.27	0.0532	0.0011	0.0490	0.0007	308.5	4.0
20.1	183	82	0.45	7.7	0.000578	0.06	20.47	0.26	0.0530	0.0009	0.0488	0.0006	307.3	3.8

Notes:

1. Uncertainties given at the one σ level
2. Error in Temora reference zircon calibration was 0.42% for the analytical session (not included in above errors but required when comparing data from different mounts).
3. f_{206} % denotes the percentage of ^{206}Pb that is common Pb.
4. Correction for common Pb for the U-Pb data has been made using the measured ^{238}U/^{206}Pb and ^{207}Pb/^{206}Pb ratios following Tera and Wasserburg (1972) as outlined in Williams (1998).

APPENDIX 1c. SUMMARY OF SHRIMP U-Pb RESULTS FOR ZIRCON FROM SAMPLE FO10-08, ALCONES.

							Total				Radiogenic		Age (Ma)	
Grain. spot	U (ppm)	Th (ppm)	Th/U	^{206}Pb* (ppm)	^{204}Pb/ ^{206}Pb	f_{206} %	^{238}U/ ^{206}Pb	±	^{207}Pb/ ^{206}Pb	±	^{206}Pb/ ^{238}U	±	^{206}Pb/ ^{238}U	±
1.1	812	409	0.50	36.7	0.000091	0.01	19.00	0.21	0.0532	0.0006	0.0526	0.0006	330.6	3.6
1.2	620	300	0.48	25.9	0.000051	0.16	20.59	0.23	0.0538	0.0006	0.0485	0.0005	305.3	3.3
2.1	554	149	0.27	24.8	0.000157	<0.01	19.20	0.22	0.0527	0.0007	0.0521	0.0006	327.4	3.6
3.1	536	180	0.34	22.9	0.000169	0.06	20.14	0.23	0.0531	0.0007	0.0496	0.0006	312.2	3.5
4.1	575	157	0.27	25.3	0.000118	0.05	19.51	0.22	0.0532	0.0006	0.0512	0.0006	322.1	3.7
5.1	1,014	495	0.49	43.8	-	0.10	19.89	0.21	0.0535	0.0005	0.0502	0.0005	316.0	3.3
6.1	476	199	0.42	21.8	0.000095	0.10	18.77	0.21	0.0539	0.0008	0.0532	0.0006	334.3	3.7
7.1	403	116	0.29	17.5	0.000087	<0.01	19.77	0.23	0.0525	0.0007	0.0506	0.0006	318.2	3.7
8.1	716	51	0.07	30.8	0.000002	0.05	20.00	0.22	0.0531	0.0006	0.0500	0.0006	314.4	3.4
8.2	677	137	0.20	29.9	0.000071	<0.01	19.45	0.21	0.0523	0.0005	0.0514	0.0006	323.4	3.5
9.1	1,310	461	0.35	57.6	0.000018	0.03	19.55	0.21	0.0530	0.0004	0.0511	0.0006	321.5	3.4
10.1	982	155	0.16	44.0	0.000013	0.10	19.14	0.20	0.0538	0.0005	0.0522	0.0006	327.9	3.5
10.2	311	127	0.41	13.1	0.000214	0.15	20.42	0.25	0.0537	0.0008	0.0489	0.0006	307.7	3.7
11.1	616	221	0.36	25.9	0.000076	0.12	20.41	0.25	0.0535	0.0006	0.0489	0.0006	308.0	3.8
12.1	1,041	241	0.23	56.6	0.000029	0.07	15.79	0.19	0.0552	0.0004	0.0633	0.0008	395.6	4.7
12.2	1,680	361	0.22	78.7	0.000098	0.01	18.34	0.19	0.0534	0.0004	0.0545	0.0006	342.2	3.5
13.1	772	227	0.29	34.3	0.000054	0.03	19.36	0.21	0.0531	0.0005	0.0516	0.0006	324.6	3.5
14.1	416	158	0.38	18.2	0.000255	0.04	19.67	0.23	0.0531	0.0007	0.0508	0.0006	319.6	3.6
15.1	465	97	0.21	20.0	0.000237	0.10	19.95	0.23	0.0535	0.0007	0.0501	0.0006	315.0	3.5
16.1	720	257	0.36	31.1	0.000099	<0.01	19.88	0.22	0.0526	0.0005	0.0503	0.0006	316.5	3.4
17.1	658	255	0.39	28.8	0.000118	<0.01	19.62	0.22	0.0524	0.0006	0.0510	0.0006	320.6	3.5
18.1	854	288	0.34	37.9	0.000114	0.11	19.36	0.21	0.0538	0.0005	0.0516	0.0006	324.3	3.4

Notes:

1. Uncertainties given at the one σ level.
2. Error in Temora reference zircon calibration was 0.39% for the analytical session (not included in above errors but required when comparing data from different mounts).
3. f_{206} % denotes the percentage of ^{206}Pb that is common Pb.
4. Correction for common Pb for the U-Pb data has been made using the measured ^{238}U/^{206}Pb and ^{207}Pb/^{206}Pb ratios following Tera and Wasserburg (1972) as outlined in Williams (1998).

APPENDIX 1d. SUMMARY OF SHRIMP U-Pb RESULTS FOR ZIRCON FROM SAMPLE FO10-20, GRANITE, LLONGOCURA.

							Total				Radiogenic		Age (Ma)	
Grain. spot	U (ppm)	Th (ppm)	Th/U	$^{206}Pb^*$ (ppm)	$^{204}Pb/^{206}Pb$	f_{206} %	$^{238}U/^{206}Pb$	±	$^{207}Pb/^{206}Pb$	±	$^{206}Pb/^{238}U$	±	$^{206}Pb/^{238}U$	±
1.1	872	289	0.33	35.8	0.000056	0.03	20.91	0.22	0.0526	0.0004	0.0478	0.0005	301.1	3.1
2.1	136	36	0.26	5.7	0.000542	0.09	20.66	0.27	0.0531	0.0011	0.0484	0.0006	304.5	4.0
3.1	321	104	0.33	13.4	0.000372	<0.01	20.65	0.24	0.0523	0.0007	0.0484	0.0006	304.9	3.5
4.1	642	246	0.38	26.7	0.000119	0.05	20.70	0.22	0.0528	0.0005	0.0483	0.0005	303.9	3.2
5.1	629	232	0.37	25.7	0.000174	0.15	21.04	0.23	0.0535	0.0005	0.0475	0.0005	298.9	3.2
6.1	198	94	0.47	8.2	0.000456	0.22	20.73	0.26	0.0541	0.0009	0.0481	0.0006	303.1	3.7
7.1	457	249	0.55	18.8	0.000124	0.20	20.86	0.23	0.0539	0.0006	0.0478	0.0005	301.2	3.3
8.1	321	110	0.34	13.0	0.000060	0.19	21.15	0.24	0.0538	0.0007	0.0472	0.0005	297.3	3.4
9.1	417	279	0.67	17.0	0.000117	0.23	21.08	0.24	0.0541	0.0006	0.0473	0.0005	298.1	3.3
10.1	807	287	0.36	33.3	0.000211	0.04	20.82	0.23	0.0527	0.0005	0.0480	0.0005	302.3	3.2
11.1	648	327	0.50	26.5	0.000122	0.05	21.00	0.23	0.0527	0.0005	0.0476	0.0005	299.8	3.2
12.1	359	123	0.34	14.6	0.000265	0.12	21.17	0.24	0.0532	0.0007	0.0472	0.0005	297.2	3.3
13.1	680	265	0.39	27.6	0.000099	0.02	21.20	0.23	0.0524	0.0005	0.0472	0.0005	297.1	3.2
14.1	262	79	0.30	10.8	0.000557	0.13	20.93	0.25	0.0534	0.0008	0.0477	0.0006	300.5	3.5
15.1	430	149	0.35	17.9	0.000284	0.12	20.57	0.23	0.0535	0.0006	0.0486	0.0005	305.6	3.4
16.1	503	168	0.33	20.7	0.000110	0.13	20.90	0.23	0.0534	0.0006	0.0478	0.0005	301.0	3.3
17.1	569	268	0.47	23.0	0.000170	0.05	21.22	0.23	0.0527	0.0006	0.0471	0.0005	296.6	3.2
18.1	533	250	0.47	22.4	0.000148	<0.01	20.45	0.22	0.0522	0.0006	0.0489	0.0005	307.8	3.3
19.1	439	196	0.45	16.7	0.000255	0.08	22.59	0.26	0.0525	0.0007	0.0442	0.0005	279.0	3.1
20.1	813	280	0.34	33.0	0.000085	0.05	21.13	0.22	0.0527	0.0004	0.0473	0.0005	297.9	3.1

Notes:

1. Uncertainties given at the one σ level.
2. Error in Temora reference zircon calibration was 0.63% for the analytical session (not included in above errors but required when comparing data from different mounts).
3. f_{206} % denotes the percentage of ^{206}Pb that is common Pb.
4. Correction for common Pb for the U-Pb data has been made using the measured $^{238}U/^{206}Pb$ and $^{207}Pb/^{206}Pb$ ratios following Tera and Wasserburg (1972) as outlined in Williams (1998).

APPENDIX 1e. SUMMARY OF SHRIMP U-Pb RESULTS FOR ZIRCON FROM SAMPLE FO09-59, CULLÍN.

							Total				Radiogenic		Age (Ma)	
Grain. spot	U (ppm)	Th (ppm)	Th/U	^{206}Pb* (ppm)	^{204}Pb/ ^{206}Pb	f_{206} %	^{238}U/ ^{206}Pb	±	^{207}Pb/ ^{206}Pb	±	^{206}Pb/ ^{238}U	±	^{206}Pb/ ^{238}U	±
1.1	225	77	0.34	9.6	0.000326	<0.01	20.22	0.28	0.0525	0.0011	0.0495	0.0007	311.3	4.2
2.1	191	64	0.33	8.3	0.001732	3.26	19.77	0.26	0.0787	0.0024	0.0489	0.0007	308.0	4.1
3.1	439	289	0.66	18.4	-	0.14	20.51	0.24	0.0536	0.0007	0.0487	0.0006	306.5	3.5
4.1	523	271	0.52	21.9	0.000103	<0.01	20.50	0.23	0.0522	0.0006	0.0488	0.0006	307.1	3.4
5.1	185	60	0.32	7.9	-	0.29	20.14	0.27	0.0549	0.0011	0.0495	0.0007	311.6	4.1
6.1	164	51	0.31	7.1	0.000292	<0.01	19.70	0.27	0.0518	0.0011	0.0508	0.0007	319.6	4.3
7.1	223	70	0.32	9.5	0.000338	0.15	20.06	0.25	0.0538	0.0010	0.0498	0.0006	313.1	3.9
8.1	176	57	0.32	7.6	-	<0.01	19.89	0.26	0.0524	0.0011	0.0503	0.0007	316.3	4.2
9.1	201	53	0.27	8.4	0.000312	0.26	20.65	0.27	0.0545	0.0010	0.0483	0.0006	304.0	3.9
10.1	165	48	0.29	6.9	0.000276	0.05	20.61	0.28	0.0528	0.0011	0.0485	0.0007	305.3	4.1
11.1	214	67	0.32	9.2	0.000270	0.07	20.07	0.26	0.0532	0.0010	0.0498	0.0006	313.2	4.0
12.1	388	249	0.64	16.7	0.000130	0.03	20.02	0.23	0.0529	0.0007	0.0499	0.0006	314.2	3.6
13.1	288	170	0.59	12.2	0.000066	0.06	20.33	0.25	0.0530	0.0008	0.0492	0.0006	309.3	3.7
14.1	160	55	0.34	6.7	0.000175	0.17	20.51	0.28	0.0538	0.0011	0.0487	0.0007	306.3	4.1
14.2	372	76	0.20	16.0	-	<0.01	19.99	0.23	0.0527	0.0008	0.0500	0.0006	314.7	3.6
15.1	179	73	0.41	7.5	0.000255	0.01	20.48	0.27	0.0526	0.0011	0.0488	0.0007	307.3	4.0
16.1	227	80	0.35	9.4	0.000083	0.23	20.66	0.26	0.0543	0.0010	0.0483	0.0006	304.0	3.8
17.1	322	108	0.34	14.2	0.000174	<0.01	19.44	0.24	0.0516	0.0008	0.0515	0.0006	323.8	4.0
18.1	339	77	0.23	14.6	-	0.17	19.97	0.32	0.0540	0.0008	0.0500	0.0008	314.5	4.9
18.2	217	43	0.20	9.3	-	<0.01	20.13	0.26	0.0524	0.0010	0.0497	0.0006	312.7	4.0
19.1	248	77	0.31	10.5	0.000116	0.09	20.33	0.25	0.0533	0.0009	0.0492	0.0006	309.3	3.8
20.1	184	56	0.31	8.0	0.000356	0.06	19.76	0.26	0.0532	0.0010	0.0506	0.0007	318.1	4.1

Notes:

1. Uncertainties given at the one σ level.
2. Error in Temora reference zircon calibration was 0.39% for the analytical session (not included in above errors but required when comparing data from different mounts).
3. f_{206} % denotes the percentage of ^{206}Pb that is common Pb.
4. Correction for common Pb for the U-Pb data has been made using the measured ^{238}U/^{206}Pb and ^{207}Pb/^{206}Pb ratios following Tera and Wasserburg (1972) as outlined in Williams (1998).

APPENDIX 1f. SUMMARY OF SHRIMP U-Pb RESULTS FOR ZIRCON FROM SAMPLE FO09-54, TRES PINOS.

							Total				Radiogenic		Age (Ma)	
Grain. spot	**U (ppm)**	**Th (ppm)**	**Th/U**	**^{206}Pb* (ppm)**	**^{204}Pb/ ^{206}Pb**	**f_{206} %**	**^{238}U/ ^{206}Pb**	**±**	**^{207}Pb/ ^{206}Pb**	**±**	**^{206}Pb/ ^{238}U**	**±**	**^{206}Pb/ ^{238}U**	**±**
1.1	708	253	0.36	29.6	0.000046	0.12	20.52	0.22	0.0534	0.0005	0.0487	0.0005	306.3	3.2
2.1	839	234	0.28	35.5	0.000042	0.08	20.33	0.23	0.0532	0.0004	0.0492	0.0006	309.4	3.5
3.1	526	294	0.56	22.4	0.000020	0.01	20.18	0.22	0.0527	0.0005	0.0495	0.0005	311.7	3.3
4.1	579	152	0.26	25.0	0.000017	<0.01	19.87	0.23	0.0517	0.0005	0.0504	0.0006	316.8	3.7
5.1	1,059	394	0.37	43.8	0.000013	0.07	20.74	0.23	0.0530	0.0004	0.0482	0.0005	303.3	3.3
6.1	381	173	0.45	16.4	0.000010	0.07	19.97	0.22	0.0532	0.0006	0.0500	0.0006	314.8	3.4
7.1	573	266	0.46	24.5	0.000006	0.06	20.13	0.22	0.0531	0.0005	0.0496	0.0005	312.3	3.3
8.1	573	179	0.31	24.1	0.000052	0.06	20.47	0.26	0.0530	0.0005	0.0488	0.0006	307.3	3.8
9.1	302	107	0.36	12.9	0.000035	0.11	20.16	0.23	0.0534	0.0007	0.0495	0.0006	311.7	3.5
10.1	214	56	0.26	8.9	0.000169	0.43	20.65	0.24	0.0559	0.0014	0.0482	0.0006	303.6	3.6
11.1	246	50	0.20	10.4	-	0.09	20.38	0.24	0.0533	0.0008	0.0490	0.0006	308.5	3.5
12.1	864	244	0.28	36.4	-	0.01	20.39	0.21	0.0526	0.0004	0.0490	0.0005	308.6	3.2
13.1	442	156	0.35	19.0	0.000064	<0.01	20.02	0.22	0.0526	0.0006	0.0499	0.0006	314.2	3.4
14.1	485	191	0.39	20.1	0.000059	<0.01	20.72	0.23	0.0524	0.0006	0.0483	0.0005	303.8	3.3
15.1	457	142	0.31	19.6	0.000067	<0.01	20.06	0.22	0.0522	0.0006	0.0499	0.0005	313.8	3.4
16.1	387	78	0.20	16.5	0.000062	<0.01	20.22	0.22	0.0523	0.0006	0.0495	0.0006	311.3	3.4
17.1	1851	617	0.33	77.6	0.000233	0.39	20.48	0.21	0.0556	0.0003	0.0486	0.0005	306.2	3.1
18.1	469	149	0.32	19.4	0.000023	<0.01	20.75	0.24	0.0521	0.0007	0.0482	0.0006	303.5	3.4
19.1	416	201	0.48	16.3	0.000640	0.75	21.87	0.25	0.0580	0.0008	0.0454	0.0005	286.1	3.2
20.1	447	140	0.31	18.9	0.000033	0.27	20.31	0.23	0.0547	0.0007	0.0491	0.0006	309.0	3.4

Notes:

1. Uncertainties given at the one σ level.
2. Error in Temora reference zircon calibration was 0.29% for the analytical session (not included in above errors but required when comparing data from different mounts).
3. f_{206} % denotes the percentage of ^{206}Pb that is common Pb.
4. Correction for common Pb for the U-Pb data has been made using the measured ^{238}U/^{206}Pb and ^{207}Pb/^{206}Pb ratios following Tera and Wasserburg (1972) as outlined in Williams (1998).

APPENDIX 1g. SUMMARY OF SHRIMP U-Pb RESULTS FOR ZIRCON FROM SAMPLE FO09-53, ANTIHUALA.

							Total				Radiogenic		Age (Ma)	
Grain. spot	**U (ppm)**	**Th (ppm)**	**Th/U**	**^{206}Pb* (ppm)**	**^{204}Pb/ ^{206}Pb**	**f_{206} %**	**^{238}U/ ^{206}Pb**	**±**	**^{207}Pb/ ^{206}Pb**	**±**	**^{206}Pb/ ^{238}U**	**±**	**^{206}Pb/ ^{238}U**	**±**
1.1	897	469	0.52	37.5	0.000424	0.48	20.53	0.22	0.0563	0.0007	0.0485	0.0005	305.1	3.3
1.2	415	419	1.01	17.9	0.000064	0.20	19.91	0.23	0.0543	0.0007	0.0501	0.0006	315.3	3.6
2.1	365	229	0.63	15.7	0.000304	0.17	20.05	0.24	0.0540	0.0008	0.0498	0.0006	313.3	3.7
3.1	448	222	0.49	19.2	0.000264	0.17	20.05	0.24	0.0540	0.0008	0.0498	0.0006	313.2	3.7
4.1	386	191	0.49	16.3	0.000121	0.22	20.29	0.25	0.0544	0.0009	0.0492	0.0006	309.5	3.7
5.1	589	340	0.58	25.5	0.000142	<0.01	19.83	0.23	0.0520	0.0007	0.0505	0.0006	317.4	3.6
6.1	851	381	0.45	36.7	0.000153	0.12	19.91	0.22	0.0536	0.0006	0.0502	0.0006	315.5	3.4
7.1	389	82	0.21	15.9	0.000132	0.22	21.00	0.26	0.0541	0.0009	0.0475	0.0006	299.2	3.6
8.1	505	350	0.69	21.4	0.000237	0.18	20.22	0.24	0.0540	0.0008	0.0494	0.0006	310.6	3.6
9.1	308	105	0.34	13.1	-	0.26	20.22	0.25	0.0547	0.0010	0.0493	0.0006	310.4	3.9
10.1	846	446	0.53	35.7	0.000051	0.04	20.39	0.22	0.0529	0.0005	0.0490	0.0005	308.5	3.3
10.2	774	380	0.49	32.3	-	0.13	20.60	0.23	0.0535	0.0007	0.0485	0.0005	305.1	3.4
11.1	407	181	0.45	17.2	0.000152	<0.01	20.35	0.24	0.0524	0.0008	0.0492	0.0006	309.4	3.6
12.1	3937	3311	0.84	147.1	0.002002	3.87	22.99	0.24	0.0825	0.0011	0.0418	0.0004	264.1	2.7
12.2	755	410	0.54	31.9	0.000163	0.03	20.36	0.26	0.0528	0.0006	0.0491	0.0006	309.0	3.9
13.1	528	388	0.73	21.9	0.000173	0.27	20.66	0.24	0.0546	0.0007	0.0483	0.0006	303.8	3.4
14.1	426	191	0.45	18.0	0.000220	0.05	20.34	0.24	0.0529	0.0008	0.0491	0.0006	309.2	3.6
15.1	1116	137	0.12	44.5	0.000322	0.48	21.57	0.23	0.0560	0.0005	0.0461	0.0005	290.7	3.1
15.2	555	256	0.46	23.6	0.000142	0.16	20.19	0.23	0.0539	0.0007	0.0494	0.0006	311.1	3.5
16.1	1064	609	0.57	44.2	0.000051	0.08	20.68	0.22	0.0531	0.0005	0.0483	0.0005	304.2	3.2
17.1	334	162	0.49	14.2	0.000264	0.04	20.18	0.25	0.0529	0.0009	0.0495	0.0006	311.7	3.8
18.1	2621	1908	0.73	112.5	0.000092	0.25	20.01	0.21	0.0546	0.0003	0.0498	0.0005	313.6	3.2

Notes:

1. Uncertainties given at the one σ level.
2. Error in Temora reference zircon calibration was 0.53% for the analytical session (not included in above errors but required when comparing data from different mounts).
3. f_{206} % denotes the percentage of ^{206}Pb that is common Pb.
4. Correction for common Pb for the U-Pb data has been made using the measured ^{238}U/^{206}Pb and ^{207}Pb/^{206}Pb ratios following Tera and Wasserburg (1972) as outlined in Williams (1998).

APPENDIX 1h. SUMMARY OF SHRIMP U-Pb RESULTS FOR ZIRCON FROM SAMPLE FO09-38, ILIHUE.

							Total				Radiogenic		Age (Ma)	
Grain. spot	U (ppm)	Th (ppm)	Th/U	$^{206}Pb^*$ (ppm)	$^{204}Pb/^{206}Pb$	f_{206} %	$^{238}U/^{206}Pb$	±	$^{207}Pb/^{206}Pb$	±	$^{206}Pb/^{238}U$	±	$^{206}Pb/^{238}U$	±
1.1	186	95	0.51	7.8	0.000335	0.21	20.45	0.29	0.0542	0.0013	0.0488	0.0007	307.2	4.3
1.2	200	88	0.44	8.7	0.000275	0.02	19.82	0.27	0.0529	0.0011	0.0504	0.0007	317.3	4.3
2.1	395	171	0.43	16.2	0.000056	0.15	20.98	0.25	0.0536	0.0008	0.0476	0.0006	299.7	3.5
2.2	224	198	0.89	9.3	0.000296	0.26	20.72	0.27	0.0545	0.0011	0.0481	0.0006	303.1	4.0
3.1	158	83	0.53	6.5	0.000504	0.18	20.93	0.30	0.0538	0.0013	0.0477	0.0007	300.4	4.3
3.2	191	157	0.83	8.0	0.000271	0.35	20.39	0.28	0.0554	0.0012	0.0489	0.0007	307.6	4.2
4.1	201	92	0.46	8.6	0.000382	<0.01	20.15	0.27	0.0525	0.0011	0.0496	0.0007	312.2	4.2
5.1	132	96	0.73	5.5	0.000974	0.19	20.59	0.31	0.0540	0.0014	0.0485	0.0007	305.2	4.5
6.1	68	34	0.50	2.8	0.000794	0.64	20.77	0.38	0.0575	0.0024	0.0478	0.0009	301.2	5.6
7.1	80	37	0.46	3.4	0.000392	0.38	20.07	0.35	0.0557	0.0018	0.0496	0.0009	312.4	5.4
8.1	209	178	0.85	8.7	0.000708	0.21	20.60	0.28	0.0541	0.0011	0.0484	0.0007	304.9	4.0
9.1	91	51	0.56	3.8	0.000324	0.19	20.35	0.34	0.0540	0.0017	0.0491	0.0008	308.7	5.1
10.1	134	69	0.51	5.7	0.000402	0.48	20.09	0.30	0.0565	0.0014	0.0495	0.0007	311.7	4.6
11.1	132	97	0.73	5.5	0.000142	0.37	20.58	0.31	0.0554	0.0014	0.0484	0.0007	304.7	4.5
12.1	537	216	0.40	22.2	0.000069	0.24	20.80	0.24	0.0543	0.0007	0.0480	0.0006	302.0	3.4
12.2	272	180	0.66	11.4	0.000280	0.22	20.51	0.27	0.0543	0.0011	0.0487	0.0006	306.2	4.0
13.1	171	96	0.56	7.1	0.000909	0.43	20.76	0.30	0.0559	0.0013	0.0480	0.0007	301.9	4.3
13.2	97	61	0.63	4.0	0.001029	0.91	20.60	0.34	0.0597	0.0017	0.0481	0.0008	302.9	4.9
14.1	165	86	0.52	7.1	0.000748	0.34	20.03	0.28	0.0553	0.0013	0.0498	0.0007	313.0	4.4
14.2	47	35	0.74	7.4	0.001380	0.63	5.382	0.095	0.0812	0.0015	0.1846	0.0034	1092	19
15.1	115	65	0.56	4.8	0.000415	0.29	20.50	0.32	0.0548	0.0016	0.0486	0.0008	306.2	4.7
16.1	110	59	0.53	4.6	0.001461	0.13	20.72	0.33	0.0535	0.0016	0.0482	0.0008	303.4	4.8
17.1	114	63	0.55	4.9	0.001542	0.50	20.07	0.31	0.0567	0.0016	0.0496	0.0008	312.0	4.8
18.1	134	107	0.80	5.7	0.001206	<0.01	20.20	0.30	0.0525	0.0014	0.0495	0.0007	311.5	4.6

Notes:
1. Uncertainties given at the one σ level.
2. Error in Temora reference zircon calibration was 0.53% for the analytical session (not included in above errors but required when comparing data from different mounts).
3. f_{206} % denotes the percentage of ^{206}Pb that is common Pb.
4. Correction for common Pb for the U-Pb data has been made using the measured $^{238}U/^{206}Pb$ and $^{207}Pb/^{206}Pb$ ratios following Tera and Wasserburg (1972) as outlined in Williams (1998).

APPENDIX 1i. SUMMARY OF SHRIMP U-Pb RESULTS FOR ZIRCON FROM SAMPLE FO09-205, QUINTAY.

							Total				Radiogenic		Age (Ma)	
Grain. spot	U (ppm)	Th (ppm)	Th/U	$^{206}Pb^*$ (ppm)	$^{204}Pb/^{206}Pb$	f_{206} %	$^{238}U/^{206}Pb$	±	$^{207}Pb/^{206}Pb$	±	$^{206}Pb/^{238}U$	±	$^{206}Pb/^{238}U$	±
1.1	155	101	0.65	3.6	0.001463	0.85	37.39	0.53	0.0562	0.0015	0.0265	0.0004	168.7	2.4
2.1	145	69	0.47	3.3	0.002378	1.49	37.30	0.54	0.0613	0.0016	0.0264	0.0004	168.1	2.4
3.1	114	84	0.74	2.6	0.002021	1.42	37.88	0.58	0.0607	0.0018	0.0260	0.0004	165.6	2.6
4.1	77	55	0.71	1.7	0.002376	2.42	37.91	0.67	0.0686	0.0024	0.0257	0.0005	163.8	2.9
5.1	118	52	0.44	2.8	0.003112	1.45	36.81	0.57	0.0610	0.0018	0.0268	0.0004	170.3	2.6
6.1	139	84	0.61	3.2	0.002055	0.99	36.64	0.54	0.0574	0.0016	0.0270	0.0004	171.9	2.5
7.1	173	114	0.66	4.0	0.002311	0.80	37.41	0.52	0.0558	0.0014	0.0265	0.0004	168.7	2.3
8.1	105	46	0.44	2.5	0.002501	1.37	36.03	0.57	0.0605	0.0019	0.0274	0.0004	174.1	2.8
9.1	81	68	0.84	1.9	0.002112	2.66	36.20	0.63	0.0707	0.0024	0.0269	0.0005	171.1	3.0
10.1	126	61	0.49	2.8	0.000956	1.45	37.94	0.57	0.0610	0.0017	0.0260	0.0004	165.3	2.5
11.1	262	253	0.96	6.0	0.001467	0.94	37.25	0.47	0.0569	0.0012	0.0266	0.0003	169.2	2.1
12.1	55	25	0.45	1.3	0.003367	2.82	36.95	0.74	0.0719	0.0029	0.0263	0.0005	167.4	3.4
13.1	187	153	0.82	4.2	0.000526	1.06	37.96	0.52	0.0578	0.0014	0.0261	0.0004	165.9	2.3
14.1	217	137	0.63	5.0	0.001320	0.50	37.35	0.50	0.0534	0.0012	0.0266	0.0004	169.5	2.2
15.1	570	775	1.36	13.2	0.000409	0.23	36.96	0.42	0.0513	0.0008	0.0270	0.0003	171.7	1.9
16.1	127	63	0.49	3.0	0.003228	1.32	36.62	0.55	0.0600	0.0017	0.0269	0.0004	171.4	2.6
17.1	142	61	0.43	3.3	0.001666	0.65	37.37	0.55	0.0546	0.0015	0.0266	0.0004	169.2	2.5
18.1	559	706	1.26	12.7	0.000648	0.14	37.77	0.43	0.0505	0.0007	0.0264	0.0003	168.2	1.9

Notes:
1. Uncertainties given at the one σ level.
2. Error in Temora reference zircon calibration was 0.51% for the analytical session (not included in above errors but required when comparing data from different mounts).
3. f_{206} % denotes the percentage of ^{206}Pb that is common Pb.
4. Correction for common Pb for the U-Pb data has been made using the measured $^{238}U/^{206}Pb$ and $^{207}Pb/^{206}Pb$ ratios following Tera and Wasserburg (1972) as outlined in Williams (1998).

APPENDIX 2a. SUMMARY OF SHRIMP Lu-Hf AND O RESULTS FOR ZIRCON FROM SAMPLE FO10-18.

Analysis spot ID	Age (Ma)	±	$^{18}O/^{16}O$	± (10^{-7})	$\delta^{18}O$‰	± 2σ	$^{176}Hf/^{177}Hf$	± (10^{-6})	$^{176}Lu/^{177}Hf$	εHf (0)	εHf (i)	± 2σ	t_{DM2} (Ga)
1.1	303.4	3.7	0.0020387	2	6.90	0.29	0.282511	12	0.00035	-9.67	-2.99	0.43	1.42
2.1	309.7	3.8	0.0020383	2	6.73	0.29	0.282515	15	0.00086	-9.56	-2.85	0.53	1.42
3.1	311.6	4.1	0.0020394	2	7.25	0.29	0.282560	13	0.00071	-7.96	-1.17	0.47	1.31
4.1	304.7	3.6	0.0020384	2	6.76	0.29	0.282564	18	0.00101	-7.81	-1.23	0.65	1.31
5.1	309.6	4.0	0.0020388	2	6.93	0.30	0.282538	11	0.00092	-8.73	-2.04	0.40	1.37
6.1	306.4	4.1	0.0020389	2	7.01	0.30	0.282554	19	0.00082	-8.18	-1.53	0.68	1.33
7.1	316.5	3.9	0.0020389	3	7.02	0.31	0.282516	13	0.00106	-9.50	-2.68	0.45	1.41
8.1	318.5	3.5	0.0020384	2	6.75	0.29	0.282552	13	0.00137	-8.26	-1.46	0.47	1.34
9.1	311.2	3.8	0.0020381	2	6.61	0.29	0.282554	12	0.00097	-8.18	-1.46	0.43	1.33
10.1	313.6	4.3	0.0020383	2	6.68	0.30	0.282516	17	0.00111	-9.53	-2.78	0.62	1.42
11.1	313.3	4.4	0.0020384	2	6.74	0.30	0.282547	19	0.00096	-8.41	-1.64	0.66	1.35
12.1	316.3	4.0	0.0020389	2	6.99	0.29	0.282521	13	0.00117	-9.35	-2.56	0.46	1.41
14.1	310.3	4.4	0.0020395	1	7.30	0.28	0.282524	11	0.00083	-9.22	-2.49	0.38	1.40
15.1	312.6	3.9	0.0020385	2	6.82	0.30	0.282516	14	0.00079	-9.51	-2.72	0.51	1.41
16.1	315.9	4.4	0.0020388	1	6.97	0.29	0.282431	132	0.00071	-12.52	-5.64	4.67	1.60
17.1	303.6	4.1	0.0020383	3	6.71	0.31	0.282498	14	0.00061	-10.16	-3.53	0.51	1.46
18.1	315.7	3.7	0.0020390	2	7.04	0.29	0.282550	13	0.00093	-8.31	-1.48	0.45	1.34

Notes:

Oxygen isotope ratios normalised relative to FC1=5.4‰.

^{176}Lu decay constant of 1.865 x 10^{-11} (Soderlund *et al.,* 2004).

$^{176}Hf/^{177}Hf$ and $^{176}Lu/^{177}Hf$ of CHUR values of 0.282785 and 0.0336 (Bouvier *et al.,* 2008).

Present day depleted mantle values of $^{176}Hf/^{177}Hf$ and $^{176}Lu/^{177}Hf$ of 0.283225 and 0.0385 (Vervoort and Blichert-Toft, 1999) and the bulk earth $^{176}Lu/^{177}Hf$ value of 0.015 (Goodge and Vervoort, 2006).

APPENDIX 2b. SUMMARY OF SHRIMP Lu-Hf AND O RESULTS FOR ZIRCON FROM SAMPLE FO10-99.

Analysis spot ID	Age (Ma)	±	$^{18}O/^{16}O$	± (10^{-7})	$\delta^{18}O$‰	± 2σ	$^{176}Hf/^{177}Hf$	± (10^{-6})	$^{176}Lu/^{177}Hf$	εHf (0)	εHf (i)	± 2σ	t_{DM2} (Ga)
1.1	306.3	4.2	0.0020361	5	6.14	0.35	0.282597	18	0.00102	-6.66	-0.06	0.62	1.24
2.1	312.1	4.4	0.0020367	4	6.40	0.33	0.282578	14	0.00088	-7.33	-0.56	0.49	1.28
3.1	306.5	4.0	0.0020363	4	6.21	0.33	0.282550	13	0.00082	-8.31	-1.66	0.45	1.34
4.1	311.0	4.9	0.0020370	4	6.58	0.33	0.282572	18	0.00113	-7.55	-0.86	0.65	1.29
5.1	314.0	4.1	0.0020360	4	6.09	0.33	0.282588	13	0.00070	-6.95	-0.11	0.45	1.25
6.1	312.7	4.1	0.0020361	3	6.12	0.31	0.282552	11	0.00055	-8.25	-1.40	0.37	1.33
7.1	307.0	3.7	0.0020366	4	6.34	0.32	0.282552	16	0.00128	-8.22	-1.66	0.57	1.34
9.1	317.1	3.7	0.0020365	4	6.29	0.32	0.282551	13	0.00077	-8.26	-1.37	0.46	1.33
10.1	305.1	3.6	0.0020361	4	6.12	0.35	0.282597	20	0.00144	-6.64	-0.15	0.70	1.24
11.1	315.5	4.7	0.0020366	4	6.37	0.33	0.282581	13	0.00109	-7.22	-0.43	0.48	1.27
12.1	313.4	4.0	0.0020363	4	6.23	0.32	0.282572	11	0.00072	-7.52	-0.69	0.40	1.29
13.1	308.0	3.7	0.0020367	4	6.40	0.33	0.282559	16	0.00142	-7.98	-1.42	0.55	1.33
14.1	296.3	4.6	0.0020375	4	6.80	0.33	0.282589	20	0.00100	-6.93	-0.53	0.72	1.26
15.1	305.1	5.1	0.0020370	4	6.54	0.34	0.282552	13	0.00049	-8.24	-1.55	0.47	1.33
16.1	303.4	3.7	0.0020374	4	6.74	0.35	0.282573	13	0.00117	-7.49	-0.98	0.44	1.30
17.1	309.3	3.6	0.0020366	4	6.39	0.33	0.282582	13	0.00112	-7.19	-0.54	0.45	1.27
18.1	299.5	4.2	0.0020370	4	6.58	0.33	0.282558	12	0.00070	-8.04	-1.52	0.43	1.33
19.1	308.5	4.0	0.0020368	4	6.48	0.34	0.282548	12	0.00100	-8.38	-1.72	0.42	1.35
20.1	307.3	3.8	0.0020361	4	6.14	0.32	0.282566	12	0.00078	-7.74	-1.07	0.44	1.30

Notes:

Oxygen isotope ratios normalised relative to FC1=5.4‰.

^{176}Lu decay constant of 1.865 x 10^{-11} (Soderlund *et al.,* 2004).

$^{176}Hf/^{177}Hf$ and $^{176}Lu/^{177}Hf$ of CHUR values of 0.282785 and 0.0336 (Bouvier *et al.,* 2008).

Present day depleted mantle values of $^{176}Hf/^{177}Hf$ and $^{176}Lu/^{177}Hf$ of 0.283225 and 0.0385 (Vervoort and Blichert-Toft, 1999) and the bulk earth $^{176}Lu/^{177}Hf$ value of 0.015 (Goodge and Vervoort, 2006).

APPENDIX 2c. SUMMARY OF SHRIMP LU-HF AND O RESULTS FOR ZIRCON FROM SAMPLE FO10-08.

Analysis spot ID	Age (Ma)	±	$^{18}O/^{16}O$	± (10^{-7})	$\delta^{18}O$‰	± 2σ	$^{176}Hf/^{177}Hf$	± (10^{-6})	$^{176}Lu/^{177}Hf$	εHf (0)	εHf (i)	± 2σ	t_{DM2} (Ga)
2.1	327.4	3.6	0.0020409	4	7.84	0.48	0.282485	14	0.00103	-10.62	-3.56	0.50	1.48
3.1	312.2	3.5	0.0020395	4	7.12	0.48	0.282503	13	0.00083	-9.99	-3.21	0.48	1.44
4.1	322.1	3.7	0.0020396	4	7.21	0.48	0.282493	14	0.00093	-10.33	-3.37	0.49	1.46
6.1	334.3	3.7	0.0020390	4	6.90	0.48	0.282550	22	0.00106	-8.31	-1.11	0.78	1.33
8.1	314.4	3.4	0.0020390	5	6.90	0.49	0.282507	17	0.00168	-9.84	-3.20	0.61	1.44
8.2	323.4	3.5	0.0020378	4	6.32	0.48	0.282505	16	0.00109	-9.89	-2.93	0.58	1.43
11.1	308.0	3.8	0.0020401	4	7.45	0.48	0.282517	12	0.00104	-9.49	-2.85	0.44	1.42
12.1	395.6	4.7	0.0020381	4	6.44	0.48	0.282511	26	0.00135	-9.70	-1.25	0.90	1.39
12.2	342.2	3.5	0.0020428	5	8.79	0.51	0.282529	34	0.00109	-9.07	-1.70	1.22	1.37
14.1	319.6	3.6	0.0020388	5	6.81	0.50	-	-	-	-	-	-	-
15.1	315.0	3.5	0.0020434	4	9.05	0.48	0.282567	35	0.00112	-7.72	-0.94	1.25	1.30

Notes:

Oxygen isotope ratios normalised relative to FC1=5.4‰.

^{176}Lu decay constant of 1.865×10^{-11} (Soderlund *et al.,* 2004).

$^{176}Hf/^{177}Hf$ and $^{176}Lu/^{177}Hf$ of CHUR values of 0.282785 and 0.0336 (Bouvier *et al.,* 2008).

Present day depleted mantle values of $^{176}Hf/^{177}Hf$ and $^{176}Lu/^{177}Hf$ of 0.283225 and 0.0385 (Vervoort and Blichert-Toft, 1999) and the bulk earth $^{176}Lu/^{177}Hf$ value of 0.015 (Goodge and Vervoort, 2006).

APPENDIX 2d. SUMMARY OF SHRIMP Lu-Hf AND O RESULTS FOR ZIRCON FROM SAMPLE FO10-20.

Analysis spot ID	Age (Ma)	±	$^{18}O/^{16}O$	± (10^{-7})	$\delta^{18}O$‰	± 2σ	$^{176}Hf/^{177}Hf$	± (10^{-6})	$^{176}Lu/^{177}Hf$	εHf (0)	εHf (i)	± 2σ	t_{DM2} (Ga)
1.1	301.1	3.1	0.0020366	4	6.38	0.33	0.282543	8	0.00107	-8.55	-2.07	0.29	1.36
2.1	304.5	4.0	0.0020389	4	7.50	0.34	0.282498	12	0.00113	-10.13	-3.59	0.42	1.46
3.1	304.9	3.5	0.0020363	4	6.23	0.33	0.282555	11	0.00077	-8.14	-1.51	0.39	1.33
4.1	303.9	3.2	0.0020366	5	6.34	0.35	0.282551	10	0.00082	-8.27	-1.67	0.34	1.34
5.1	298.9	3.2	0.0020367	5	6.40	0.35	0.282537	11	0.00093	-8.78	-2.32	0.40	1.38
6.1	303.1	3.7	0.0020372	5	6.63	0.35	0.282552	10	0.00118	-8.25	-1.74	0.36	1.34
7.1	301.2	3.3	0.0020362	4	6.14	0.34	0.282558	12	0.00147	-8.03	-1.62	0.44	1.33
8.1	297.3	3.4	0.0020372	4	6.64	0.33	0.282532	11	0.00076	-8.96	-2.50	0.37	1.39
9.1	298.1	3.3	0.0020375	3	6.80	0.31	0.282562	13	0.00119	-7.88	-1.48	0.45	1.32
10.1	302.3	3.2	0.0020369	4	6.53	0.32	0.282542	14	0.00097	-8.59	-2.06	0.51	1.36
11.1	299.8	3.2	0.0020373	4	6.70	0.33	0.282530	12	0.00083	-9.00	-2.50	0.42	1.39
12.1	297.2	3.3	0.0020369	4	6.50	0.34	0.282537	10	0.00086	-8.77	-2.33	0.35	1.38
13.1	297.1	3.2	0.0020380	4	7.06	0.34	0.282547	11	0.00084	-8.41	-1.97	0.39	1.35
14.1	300.5	3.5	0.0020368	4	6.48	0.33	0.282559	11	0.00111	-7.99	-1.52	0.38	1.33
15.1	305.6	3.4	0.0020373	4	6.68	0.34	0.282558	12	0.00080	-8.04	-1.40	0.43	1.32
16.1	301.0	3.3	0.0020370	4	6.55	0.33	0.282510	11	0.00096	-9.73	-3.23	0.40	1.44
17.1	296.6	3.2	0.0020367	4	6.40	0.33	0.282538	15	0.00085	-8.74	-2.31	0.54	1.37
18.1	307.8	3.3	0.0020371	4	6.62	0.33	0.282531	18	0.00085	-8.97	-2.30	0.65	1.38
19.1	279.0	3.1	0.0020370	4	6.55	0.32	0.282545	12	0.00057	-8.49	-2.39	0.43	1.37
20.1	297.9	3.1	0.0020367	4	6.39	0.33	0.282606	22	0.00115	-6.34	0.06	0.76	1.23

Notes:

Oxygen isotope ratios normalised relative to FC1=5.4‰.

^{176}Lu decay constant of 1.865 x 10^{-11} (Soderlund *et al.,* 2004).

$^{176}Hf/^{177}Hf$ and $^{176}Lu/^{177}Hf$ of CHUR values of 0.282785 and 0.0336 (Bouvier *et al.,* 2008).

Present day depleted mantle values of $^{176}Hf/^{177}Hf$ and $^{176}Lu/^{177}Hf$ of 0.283225 and 0.0385 (Vervoort and Blichert-Toft, 1999) and the bulk earth $^{176}Lu/^{177}Hf$ value of 0.015 (Goodge and Vervoort, 2006).

APPENDIX 2e. SUMMARY OF SHRIMP Lu-Hf AND O RESULTS FOR ZIRCON FROM SAMPLE FO09-59.

Analysis spot ID	Age (Ma)	±	$^{18}O/^{16}O$	± (10^{-7})	$\delta^{18}O$‰	± 2σ	$^{176}Hf/^{177}Hf$	± (10^{-6})	$^{176}Lu/^{177}Hf$	εHf (0)	εHf (i)	± 2σ	t_{DM2} (Ga)
1.1	311.3	4.2	0.0020414	4	8.09	0.49	0.282520	20	0.00133	-9.38	-2.73	0.72	1.41
2.1	308.0	4.1	0.0020424	4	8.55	0.48	0.282493	18	0.00149	-10.32	-3.77	0.63	1.48
4.1	307.1	3.4	0.0020433	4	9.03	0.48	0.282506	17	0.00249	-9.88	-3.55	0.62	1.46
5.1	311.6	4.1	0.0020424	4	8.56	0.48	0.282488	18	0.00097	-10.52	-3.79	0.65	1.48
6.1	319.6	4.3	0.0020419	4	8.32	0.48	0.282506	16	0.00117	-9.86	-3.00	0.56	1.44
8.1	316.3	4.2	0.0020423	4	8.53	0.48	0.282482	14	0.00094	-10.71	-3.87	0.48	1.49
9.1	304.0	3.9	0.0020429	3	8.84	0.47	0.282522	31	0.00131	-9.30	-2.81	1.11	1.41
10.1	305.3	4.1	0.0020426	4	8.66	0.49	0.282503	25	0.00101	-9.99	-3.40	0.88	1.45
11.1	313.2	4.0	0.0020427	4	8.70	0.47	0.282493	16	0.00106	-10.32	-3.58	0.55	1.47
12.1	314.2	3.6	0.0020425	4	8.62	0.49	0.282540	46	0.00148	-8.66	-1.98	1.63	1.37
13.1	309.3	3.7	0.0020418	4	8.29	0.47	0.282502	33	0.00116	-10.03	-3.38	1.17	1.45
14.1	306.3	4.1	0.0020432	4	8.97	0.47	0.282574	25	0.00164	-7.47	-0.99	0.90	1.30
16.1	304.0	3.8	0.0020428	5	8.75	0.49	0.282485	21	0.00125	-10.62	-4.11	0.75	1.49
18.1	314.5	4.9	0.0020426	4	8.67	0.48	0.282502	21	0.00168	-10.01	-3.37	0.74	1.46
18.2	312.7	4.0	0.0020426	4	8.66	0.48	0.282473	13	0.00089	-11.02	-4.25	0.47	1.51

Notes:

Oxygen isotope ratios normalised relative to FC1=5.4‰.

^{176}Lu decay constant of 1.865 x 10^{-11} (Soderlund *et al.,* 2004).

$^{176}Hf/^{177}Hf$ and $^{176}Lu/^{177}Hf$ of CHUR values of 0.282785 and 0.0336 (Bouvier *et al.,* 2008).

Present day depleted mantle values of $^{176}Hf/^{177}Hf$ and $^{176}Lu/^{177}Hf$ of 0.283225 and 0.0385 (Vervoort and Blichert-Toft, 1999) and the bulk earth $^{176}Lu/^{177}Hf$ value of 0.015 (Goodge and Vervoort, 2006).

APPENDIX 2f. SUMMARY OF SHRIMP Lu-Hf AND O RESULTS FOR ZIRCON FROM SAMPLE FO09-54.

Analysis spot ID	Age (Ma)	±	$^{18}O/^{16}O$	± (10^{-7})	$\delta^{18}O$‰	± 2σ	$^{176}Hf/^{177}Hf$	± (10^{-6})	$^{176}Lu/^{177}Hf$	εHf (0)	εHf (i)	± 2σ	t_{DM2} (Ga)
1.1	306.3	3.2	0.0020339	6	6.99	0.55	0.282587	63	0.00077	-6.99	-0.34	2.23	1.26
3.1	311.7	3.3	0.0020330	5	6.54	0.52	0.282567	44	0.00141	-7.70	-1.06	1.56	1.31
4.1	316.8	3.7	0.0020359	5	7.98	0.52	0.282570	25	0.00109	-7.60	-0.77	0.88	1.29
5.1	303.3	3.3	0.0020340	5	7.00	0.52	0.282587	26	0.00116	-6.99	-0.48	0.92	1.26
6.1	314.8	3.4	0.0020352	6	7.61	0.53	0.282564	30	0.00078	-7.81	-0.97	1.06	1.30
7.1	312.3	3.3	0.0020334	6	6.72	0.53	0.282592	24	0.00107	-6.82	-0.09	0.85	1.25
8.1	307.3	3.8	0.0020336	6	6.81	0.55	0.282569	27	0.00091	-7.63	-0.98	0.96	1.30
9.1	311.7	3.5	0.0020376	5	8.82	0.53	0.282537	28	0.00167	-8.76	-2.17	0.99	1.38
10.1	303.6	3.6	0.0020347	6	7.37	0.54	0.282586	22	0.00125	-7.03	-0.53	0.78	1.27
11.1	308.5	3.5	0.0020348	5	7.43	0.52	0.282574	28	0.00062	-7.45	-0.72	0.99	1.28
13.1	314.2	3.4	0.0020358	6	7.90	0.54	0.282639	53	0.00081	-5.16	1.67	1.88	1.14
14.1	303.8	3.3	0.0020343	5	7.18	0.52	0.282547	22	0.00077	-8.41	-1.81	0.78	1.35
15.1	313.8	3.4	0.0020333	6	6.67	0.53	0.282644	27	0.00152	-4.98	1.69	0.96	1.14
16.1	311.3	3.4	0.0020355	7	7.75	0.56	0.282578	25	0.00099	-7.31	-0.59	0.88	1.28
19.1	286.1	3.2	0.0020349	7	7.44	0.56	0.282578	30	0.00088	-7.31	-1.12	1.06	1.29
20.1	309.0	3.4	0.0020352	7	7.60	0.56	0.282585	24	0.00061	-7.07	-0.32	0.85	1.26

Notes:

Oxygen isotope ratios normalised relative to FC1=5.4‰.

^{176}Lu decay constant of 1.865×10^{-11} (Soderlund *et al.,* 2004).

$^{176}Hf/^{177}Hf$ and $^{176}Lu/^{177}Hf$ of CHUR values of 0.282785 and 0.0336 (Bouvier *et al.,* 2008).

Present day depleted mantle values of $^{176}Hf/^{177}Hf$ and $^{176}Lu/^{177}Hf$ of 0.283225 and 0.0385 (Vervoort and Blichert-Toft, 1999) and the bulk earth $^{176}Lu/^{177}Hf$ value of 0.015 (Goodge and Vervoort, 2006).

APPENDIX 2g. SUMMARY OF SHRIMP Lu-Hf AND O RESULTS FOR ZIRCON FROM SAMPLE FO09-53.

Analysis spot ID	Age (Ma)	±	$^{18}O/^{16}O$	± (10^{-7})	$\delta^{18}O$‰	± 2σ	$^{176}Hf/^{177}Hf$	± (10^{-6})	$^{176}Lu/^{177}Hf$	εHf (0)	εHf (i)	± 2σ	t_{DM2} (Ga)
1.2	315.3	3.6	0.0020328	8	6.83	0.64	0.282604	29	0.00092	-6.40	0.42	1.03	1.22
2.1	313.3	3.7	0.0020338	5	7.31	0.57	0.282586	29	0.00140	-7.04	-0.36	1.03	1.26
3.1	313.2	3.7	0.0020351	7	7.95	0.61	0.282558	34	0.00070	-8.03	-1.20	1.20	1.32
4.1	309.5	3.7	0.0020355	3	8.12	0.53	0.282583	37	0.00093	-7.14	-0.45	1.31	1.27
5.1	317.4	3.6	0.0020354	7	8.06	0.61	0.282595	31	0.00077	-6.72	0.18	1.10	1.23
7.1	299.2	3.6	0.0020332	5	7.02	0.56	0.282592	29	0.00082	-6.82	-0.33	1.03	1.25
8.1	310.6	3.6	0.0020339	7	7.33	0.62	0.282568	71	0.00082	-7.67	-0.93	2.51	1.30
10.1	308.5	3.3	0.0020348	8	7.77	0.64	0.282620	38	0.00146	-5.83	0.73	1.34	1.19
12.2	309.0	3.9	0.0020361	6	8.41	0.58	0.282575	32	0.00094	-7.43	-0.74	1.13	1.29
13.1	303.8	3.4	0.0020344	2	7.58	0.52	0.282609	44	0.00091	-6.22	0.35	1.56	1.21
14.1	309.2	3.6	0.0020348	7	7.80	0.62	0.282572	40	0.00090	-7.53	-0.84	1.42	1.29
15.2	311.1	3.5	0.0020360	6	8.40	0.59	0.282600	31	0.00081	-6.54	0.21	1.10	1.23

Notes:

Oxygen isotope ratios normalised relative to FC1=5.4‰.

^{176}Lu decay constant of 1.865 x 10^{-11} (Soderlund *et al.,* 2004).

$^{176}Hf/^{177}Hf$ and $^{176}Lu/^{177}Hf$ of CHUR values of 0.282785 and 0.0336 (Bouvier *et al.,* 2008).

Present day depleted mantle values of $^{176}Hf/^{177}Hf$ and $^{176}Lu/^{177}Hf$ of 0.283225 and 0.0385 (Vervoort and Blichert-Toft, 1999) and the bulk earth $^{176}Lu/^{177}Hf$ value of 0.015 (Goodge and Vervoort, 2006).

APPENDIX 2h. SUMMARY OF SHRIMP Lu-Hf AND O RESULTS FOR ZIRCON FROM SAMPLE FO09-38.

Analysis spot ID	Age (Ma)	±	$^{18}O/^{16}O$	± (10^{-7})	$\delta^{18}O$‰	± 2σ	$^{176}Hf/^{177}Hf$	± (10^{-6})	$^{176}Lu/^{177}Hf$	εHf (0)	εHf (i)	± 2σ	t_{DM2} (Ga)
2.1	299.7	3.5	0.0020336	5	7.18	0.57	0.282573	43	0.00112	-7.50	-1.05	1.52	1.30
2.2	303.1	4.0	0.0020358	4	8.26	0.54	0.282583	30	0.00098	-7.14	-0.60	1.06	1.27
3.1	300.4	4.3	0.0020359	4	8.30	0.55	0.282564	34	0.00077	-7.82	-1.29	1.20	1.31
3.2	307.6	4.2	0.0020354	4	8.11	0.54	0.282568	37	0.00123	-7.67	-1.08	1.31	1.31
4.1	312.2	4.2	0.0020336	4	7.19	0.55	0.282597	33	0.00077	-6.65	0.14	1.17	1.23
5.1	305.2	4.5	-	-	-	-	0.282568	34	0.00109	-7.67	-1.11	1.20	1.31
6.1	301.2	5.6	0.0020357	3	8.25	0.53	0.282575	78	0.00084	-7.43	-0.89	2.76	1.29
7.1	312.4	5.4	0.0020335	5	7.16	0.57	0.282580	28	0.00068	-7.25	-0.44	0.99	1.27
10.1	311.7	4.6	0.0020338	4	7.32	0.55	0.282527	32	0.00099	-9.12	-2.40	1.13	1.39
11.1	304.7	4.5	0.0020335	5	7.13	0.57	0.282536	37	0.00078	-8.81	-2.19	1.31	1.37
13.1	301.9	4.3	0.0020343	6	7.54	0.58	0.282598	38	0.00063	-6.61	-0.02	1.34	1.23
15.1	306.2	4.7	0.0020331	6	6.98	0.60	0.282542	43	0.00085	-8.59	-1.96	1.52	1.36
17.1	312.0	4.8	0.0020344	7	7.59	0.62	0.282582	26	0.00068	-7.18	-0.38	0.92	1.26
18.1	311.5	4.6	0.0020367	6	8.71	0.59	0.282582	31	0.00056	-7.18	-0.36	1.10	1.26

Notes:

Oxygen isotope ratios normalised relative to FC1=5.4‰.

^{176}Lu decay constant of 1.865×10^{-11} (Soderlund *et al.,* 2004).

$^{176}Hf/^{177}Hf$ and $^{176}Lu/^{177}Hf$ of CHUR values of 0.282785 and 0.0336 (Bouvier *et al.,* 2008).

Present day depleted mantle values of $^{176}Hf/^{177}Hf$ and $^{176}Lu/^{177}Hf$ of 0.283225 and 0.0385 (Vervoort and Blichert-Toft, 1999) and the bulk earth $^{176}Lu/^{177}Hf$ value of 0.015 (Goodge and Vervoort, 2006).

APPENDIX 2i. SUMMARY OF SHRIMP Lu-Hf AND O RESULTS FOR ZIRCON FROM SAMPLE FO09-205.

Analysis spot ID	Age (Ma)	±	$^{18}O/^{16}O$	± (10^{-7})	$\delta^{18}O$‰	± 2σ	$^{176}Hf/^{177}Hf$	± (10^{-6})	$^{176}Lu/^{177}Hf$	εHf (0)	εHf (i)	± 2σ	t_{DM2} (Ga)
1	168.7	2.4	0.0020406	2	5.55	0.34	0.282816	17	0.00103	1.11	4.74	0.60	826
2	168.1	2.4	0.0020409	2	5.73	0.35	0.282795	14	0.00033	0.36	4.06	0.48	869
3	165.6	2.6	0.0020403	2	5.42	0.35	0.282817	19	0.00042	1.11	4.75	0.67	823
4	163.8	2.9	0.0020402	3	5.38	0.37	0.282820	18	0.00057	1.25	4.83	0.62	817
5	170.3	2.6	0.0020402	2	5.39	0.35	0.282808	16	0.00045	0.81	4.54	0.58	840
6	171.9	2.5	0.0020402	3	5.34	0.36	0.282817	15	0.00038	1.14	4.92	0.54	818
7	168.7	2.3	0.0020401	2	5.33	0.35	0.282815	18	0.00053	1.06	4.75	0.63	826
8	174.1	2.8	0.0020408	3	5.67	0.37	0.282804	18	0.00070	0.66	4.45	0.63	849
9	171.1	3.0	0.0020402	2	5.38	0.35	0.282775	19	0.00068	-0.35	3.37	0.68	915
10	165.3	2.5	-	-	-	-	0.282812	18	0.00033	0.95	4.58	0.65	834
11	169.2	2.1	0.0020401	2	5.30	0.35	0.282818	20	0.00164	1.18	4.76	0.70	825
12	167.4	3.4	0.0020401	4	5.30	0.38	0.282841	21	0.00047	2.00	5.67	0.73	767
13	165.9	2.3	0.0020389	3	4.72	0.35	0.282832	19	0.00062	1.67	5.29	0.66	789
14	169.5	2.2	0.0020404	5	5.47	0.40	0.282816	20	0.00105	1.10	4.75	0.69	827
15	171.7	1.9	0.0020403	2	5.39	0.34	0.282826	21	0.00133	1.46	5.13	0.72	804
16	171.4	2.6	0.0020396	2	5.08	0.34	0.282822	16	0.00090	1.30	5.01	0.57	811
17	169.2	2.5	0.0020398	1	5.17	0.35	0.282795	26	0.00077	0.35	4.02	0.91	872
18	168.2	1.9	0.0020394	2	4.98	0.35	0.282843	20	0.00189	2.06	5.59	0.70	772

Notes:

Oxygen isotope ratios normalised relative to FC1=5.4‰.

^{176}Lu decay constant of 1.865 x 10^{-11} (Soderlund *et al.,* 2004).

$^{176}Hf/^{177}Hf$ and $^{176}Lu/^{177}Hf$ of CHUR values of 0.282785 and 0.0336 (Bouvier *et al.,* 2008).

Present day depleted mantle values of $^{176}Hf/^{177}Hf$ and $^{176}Lu/^{177}Hf$ of 0.283225 and 0.0385 (Vervoort and Blichert-Toft, 1999) and the bulk earth $^{176}Lu/^{177}Hf$ value of 0.015 (Goodge and Vervoort, 2006).